The Black-Hole Limits of the Spherically Symmetric and Static Relativistic Polytrope Solutions

Jorge L. deLyra*

Universidade de São Paulo
Instituto de Física
Rua do Matão, 1371,
05508-090 São Paulo, SP, Brazil

July 15, 2023

Abstract

We examine the black-hole limits of the family of static and spherically symmetric exact solutions of the Einstein field equations for polytropic matter, that was presented in a previous paper. This exploration is done in the asymptotic sub-regions of the allowed regions of the parameter planes of that family of solutions, for a few values of the polytropic index n, with the limitation that $n > 1$. These allowed regions were determined and discussed in some detail in another previous paper.

The characteristics of these limits are examined and analyzed. We find that there are different types of black-hole limits, with specific characteristics, involving for example the local temperature of the matter. We also find that the limits produce a very unexpected but specific type of spacetime geometry in the interior of the black holes, which we analyze in detail. Regarding the spatial part of the geometry, we show that in the black-hole limits there is a general collapse of all radial distances to zero. Regarding the temporal part, there results an infinite overall red shift in the limits, with respect to the flat space at radial infinity, over the whole interior region.

We argue that the black-hole limits cannot actually be taken all the way to their ultimate conclusion, due to the fact that this would lead to the violation of some essential physical and mathematical conditions. These include questions of consistency of the solutions, questions involving infinite energies, and violations of the quantum behavior of matter. However, one can still approach these limiting situations to a very significant degree, from the physical standpoint, so that the limits can still be considered, at least for some purposes, as useful and simpler approximate representations of physically realizable configurations.

*Email: delyra@lmail.if.usp.br ORCID: 0000-0002-8551-9711

Keywords:
General Relativity, Einstein Equations, Polytrope Solutions, Black Holes, Event Horizons.

DOI: 10.5281/zenodo.XXXXXXX

1 Introduction

The concept of a black hole in General Relativity was introduced more that a hundred years ago, in connection to the properties of the exterior Schwarzschild solution [1], in particular in the vicinity of its event horizon. That concept has been taken seriously for more than fifty years, since about the time of the invention and popularization of the term "black hole" by Wheeler. In time it has become an universally accepted concept, and even a household name. Today there can be no doubt that astronomical objects do exist whose exterior regions are described correctly by the exterior Schwarzschild or Kerr [2] solutions. Much has also been said about the interior regions of black holes, beyond the position of the event horizon, almost all of it based on very uncertain arguments or evidence. This is due to the fact that until recently there were no significant solutions of the Einstein field equations that had the following two important properties: first, that they be valid along the whole three-dimensional spatial manifold; and second, that they allow for the consideration of limits that approach the formation of event horizons. For example, the combination of the Schwarzschild exterior and interior [3] solutions, connected by appropriate boundary conditions on an interface between two concentric spherically symmetric regions, has the first property, but not the second one.

However, a class of solutions that do have these two properties now exists, which will allow us to discuss what happens in the interior region of a black hole, or more precisely in the region of the solutions that is interior to the radial position where the event horizon will eventually come into existence, when a black-hole limit is taken, with basis on solid, explicit and precise mathematical results. Given these circumstances, it should come as no surprise that what we find in this way is entirely different from the almost universally accepted current cannons of the subject. In a previous paper [4] we established the static solution of the Einstein field equations for the case of spherically symmetric shells of gaseous polytropic fluids located between radial positions r_1 and r_2 of the Schwarzschild system of coordinates. This consists of a four-parameter family of solutions, that can be reduced to a three-parameter family of solutions when they are written in terms of dimensionless variables. The fourth parameter, which is the asymptotic gravitational mass M of the system, is essentially factored out of the system, as discussed in the subsequent paper [5], which simply means that there are solutions for all possible values of M.

In [5] the parameter space of this family of solutions was explored. For each value of the polytropic index n the solutions can be described and classified according to a parameter plane spanned by the other two dimensionless free parameters, namely the dimensionless polytropic constant C associated to the usual polytropic constant K, and the dimensionless parameter π_e that is associated to the maximum value of the matter energy density. Taking into account the condition of the mathematical existence of the solutions of the differential equations, as well as the Dominant Energy Condition (DEC) to be satisfied by the matter stress-energy tensor, certain allowed regions are defined within these (C, π_e) parameter planes. Graphs of the parameter planes showing the corresponding allowed regions can be found in [5], for a few values of n.

While these allowed regions exist within finite intervals of values of the parameter C, between zero and a maximum value of the order of one, in terms of π_e they extend all the way from $\pi_e = 0$ to $\pi_e \to \infty$. Due to the shape of the allowed regions, when we make $\pi_e \to \infty$ we must also make $C \to 0$, in order to stay within these allowed regions. These asymptotic sub-regions of the allowed regions, where π_e becomes very large and C very small, is where all the black-hole limits are to be found. These limits are characterized by the approach to the formation of an event horizon at the radial position r_2 of the outer

surface of the matter. This is indicated by the fact that in these limits the Schwarzschild radius r_M approaches the outer radius r_2 from below, thus generating at that position the well-known coordinate singularity of the exterior Schwarzschild solution.

In this paper we explore the black-hole limits of this new class of solutions, with two main objectives. First, to establish their existence, as mathematical limits, and second, to establish some of their properties, and in particular the geometrical properties of the interior regions of the black holes in these limits. This will lead us to a discussion of the issue of whether or not these limits can actually be taken, in terms of the physics involved, that is, of whether or not they lead to objects with well-defined and acceptable physical properties. As we will see, the answer to this last question turns out to be no. The limits can be approached to a certain extent, but cannot be actually taken without mathematical inconsistencies and without violating essential physical principles related to the behavior of the matter.

This paper is organized as follows: in Section 2 we review the new class of static and spherically symmetric exact solutions for gaseous shells; in Section 3 we describe the exploration of the asymptotic regions of the allowed regions of the parameter planes; in Section 4 we give the results of that exploration, and discuss these results; in Section 5 we give an analysis of the geometry of the interior of the black holes; in Section 6 we discuss the concept of singularity in General Relativity and propose a new definition of singularity; and in Section 7 we state our conclusions.

2 Review of the Polytropic Solutions

In this section we will review the solutions for gaseous fluids presented in [4], in order to establish the notation, as well as the most basic character of the solutions. Both the notation and the ideas presented in [4] rely on some of the notation and ideas presented in the previous paper [6], in which we presented the exact solution for the case of liquid fluids. In this work we will use the time-like signature $(+,-,-,-)$, following [7]. In terms of the coefficients of the metric, for a static invariant interval given in terms of the Schwarzschild coordinates (t, r, θ, ϕ) by

$$ds^2 = \mathrm{e}^{2\nu(r)}c^2dt^2 - \mathrm{e}^{2\lambda(r)}dr^2 - r^2\left[d\theta^2 + \sin^2(\theta)d\phi^2\right], \tag{1}$$

where $\exp[\nu(r)]$ and $\exp[\lambda(r)]$ are two positive functions of only r, as was explained in [6] the Einstein field equations reduce to the set of three first-order differential equations

$$\left\{1 - 2\left[r\lambda'(r)\right]\right\}\mathrm{e}^{-2\lambda(r)} = 1 - \kappa r^2\rho(r), \tag{2}$$

$$\left\{1 + 2\left[r\nu'(r)\right]\right\}\mathrm{e}^{-2\lambda(r)} = 1 + \kappa r^2 P(r), \tag{3}$$

$$\left[\rho(r) + P(r)\right]\nu'(r) = -P'(r), \tag{4}$$

where $\rho(r)$ is the energy density of the matter, $P(r)$ is its isotropic pressure, and the constant κ is given by $\kappa = 8\pi G/c^4$, where G is the universal gravitational constant and c is the speed of light. In these equations the primes indicate differentiation with respect to r. It is convenient for the analysis of the solutions to change variables in the field equations from the function $\lambda(r)$ to a function $\beta(r)$, which is defined to be such that

$$\mathrm{e}^{2\lambda(r)} = \frac{r}{r - r_M\beta(r)}, \tag{5}$$

where $r_M = 2GM/c^2$ is the Schwarzschild radius associated to the total asymptotic gravitational mass M, which then implies that we have for the corresponding derivatives

$$2r\lambda'(r) = -r_M \, \frac{\beta(r) - r\beta'(r)}{r - r_M\beta(r)}. \tag{6}$$

Substituting the expressions in Equations (5) and (6) in the component field equation shown in Equation (2) a very simple relation giving the derivative of $\beta(r)$ in terms of $\rho(r)$ results,

$$\beta'(r) = \frac{\kappa r^2 \rho(r)}{r_M}. \tag{7}$$

Therefore, in any interval where $\rho(r) = 0$ we have that $\beta(r)$ is a constant. Since we must have that $\rho(r) \geq 0$, it therefore follows that $\beta(r)$ is a monotonically increasing function, which is a constant if and only if we are within a vacuum region. In addition to this, since according to the asymptotic boundary condition we must have that $\beta(r) \to 1$ when $r \to \infty$, it also follows that $\beta(r)$ is limited from above by 1.

In the previous paper [4] we established the static solution of the Einstein field equations for the case of a spherically symmetric shell of gaseous fluid located between the radial positions r_1 and r_2 of the Schwarzschild system of coordinates. These positions are *not* arbitrary, but rather are obtained as part of the solution of the problem. For this problem we assume the hypothesis that the gas satisfies the polytropic equation of state

$$P(r) = K \left[\rho(r)\right]^{1+1/n}, \tag{8}$$

where K, the polytropic constant, is a positive real constant, and $n > 1$, the polytropic index, is a real number that, merely for simplicity, may be taken to be an integer or half-integer. For convenience we define the auxiliary quantity

$$F(r) = K \left[\rho(r)\right]^{1/n}, \tag{9}$$

in terms of which the equation of state becomes simply

$$P(r) = F(r)\rho(r). \tag{10}$$

As was shown in [4], given the field Equations (2) through (4) and the equation of state shown in Equation (8), the solution for $\lambda(r)$ is given by

$$\lambda(r) \;=\; \begin{cases} -\dfrac{1}{2}\,\ln\!\left(\dfrac{r + r_\mu}{r}\right) & \text{for} \quad 0 \;< r \leq r_1, \\ -\dfrac{1}{2}\,\ln\!\left[\dfrac{r - r_M\beta(r)}{r}\right] & \text{for} \quad r_1 \leq r \leq r_2, \\ -\dfrac{1}{2}\,\ln\!\left(\dfrac{r - r_M}{r}\right) & \text{for} \quad r_2 \leq r < \infty, \end{cases} \tag{11}$$

where once more $r_M = 2GM/c^2$, while for $\nu(r)$ we have

$$\nu(r) \;=\; \begin{cases} \dfrac{1}{2}\,\ln\!\left(\dfrac{1 - r_M/r_2}{1 + r_\mu/r_1}\right) + \dfrac{1}{2}\,\ln\!\left(\dfrac{r + r_\mu}{r}\right) & \text{for} \quad 0 \;< r \leq r_1, \\ \nu(r_2) - (n+1)\ln[1 + F(r)] & \text{for} \quad r_1 \leq r \leq r_2, \\ \dfrac{1}{2}\,\ln\!\left(\dfrac{r - r_M}{r}\right) & \text{for} \quad r_2 \leq r < \infty. \end{cases} \tag{12}$$

The solution introduces into the system, through the interface boundary conditions, the new physical parameter r_μ with dimensions of length, which can be associated to a mass parameter μ in the same way that r_M is associated to M, namely by $r_\mu = 2G\mu/c^2$. As was also shown in [4], the determination of the function $\beta(r)$ in the matter region leads with no further difficulty to the determination of all the functions that describe both the matter and the geometry of the system within that region, by means of the exact analytical relations

$$\rho(r) = \frac{r_M \beta'(r)}{\kappa r^2}, \tag{13}$$

$$P(r) = K\left[\frac{r_M \beta'(r)}{\kappa r^2}\right]^{1+1/n}, \tag{14}$$

$$F(r) = K\left[\frac{r_M \beta'(r)}{\kappa r^2}\right]^{1/n}, \tag{15}$$

$$\lambda(r) = \frac{1}{2}\ln\left[\frac{r}{r - r_M\beta(r)}\right], \tag{16}$$

$$\nu(r) = \nu(r_2) - (n+1)\ln[1 + F(r)]. \tag{17}$$

This also determines the solutions within the inner and outer vacuum regions, which depend only on r_μ and r_M, through the interface boundary conditions at r_1 and r_2. The four free parameters of the system are K, n and M, all of which describe the nature and state of the matter, and the value of $\beta'(r)$ at its point of maximum, which can also be seen to be related to the matter, since it determines the general scale of the matter energy density, as can be seen from Equation (7). Note that the radial positions r_1 and r_2 are not chosen by hand, but are instead defined as the positions where the matter energy density $\rho(r)$ becomes zero. As was shown in [4], this differential system has the property that once $\rho(r)$ hits the value zero during the integration, in either direction, it stays at zero from that point on, thus generating a vacuum region.

For all sets of parameters for which there is a solution of the differential problem the function $\beta'(r)$ has a single point of maximum within the matter region, which is the point where $\beta(r)$ has its single inflection point. As was also shown in [4], for all existing solutions with $r_1 > 0$ it holds that $r_\mu > 0$. This in turn implies that $\beta(r)$ has a single zero within the matter region. The strictly positive value of r_μ implies that the solutions have singularities at the origin. However, that type of singularity, although it has the invariant character of a curvature singularity, has also a repulsive rather than attractive character, and thus is not associated to an infinite concentration of matter, but rather, as explained in [6], to exactly zero matter energy density at that point, as well as in its neighborhood.

Both for the subsequent analysis and for the numerical approach, it is convenient to further transform variables at this point, in order to write everything in terms of dimensionless variables and functions. In order to do this we must now introduce an arbitrary radial reference position $r_0 > 0$. For now the value of this parameter remains completely arbitrary, other than that it must be strictly positive, and has no particular physical meaning. It is only a mathematical device that allows us to define a dimensionless radial variable and a dimensionless parameter associated to the mass M by

$$\xi = \frac{r}{r_0}, \tag{18}$$

$$\xi_M = \frac{r_M}{r_0}, \tag{19}$$

as well as to define the dimensionless function of ξ, meant to assume the role of $\beta(r)$,

$$\gamma(\xi) = \xi_M \beta(r). \tag{20}$$

Note that the asymptotic condition that $\beta(r) \to 1$ for sufficiently large r translates here as the condition that $\gamma(\xi) \to \xi_M$ for sufficiently large ξ. Note also that, since $\beta(r)$ is a limited monotonic function, it follows from Equation (20) that $\gamma(\xi)$ is also a monotonically increasing function which is limited from above by the parameter ξ_M. We also have that $\gamma(\xi)$ is constant within vacuum regions. As was shown in [4] the functions $\gamma(\xi)$ and $\beta(r)$ are both determined by the second-order ordinary differential equation

$$\pi'(\xi) = \pi(\xi) \left\{ \frac{2}{\xi} - \frac{n}{n+1} \frac{1}{\xi - \gamma(\xi)} \frac{1 + F(\xi,\pi)}{2F(\xi,\pi)} \left[\frac{\gamma(\xi)}{\xi} + F(\xi,\pi)\pi(\xi) \right] \right\}, \tag{21}$$

where $\pi(\xi) = \gamma'(\xi)$ is the derivative of $\gamma(\xi)$, the primes now indicate derivatives with respect to ξ, and $F(\xi,\pi)$ is given by

$$F(\xi,\pi) = C \left[\frac{\pi(\xi)}{\xi^2} \right]^{1/n}, \tag{22}$$

where $C = K/\left(\kappa r_0^2\right)^{1/n}$ is a dimensionless constant associated to the polytropic constant K. This differential system can be interpreted either as a second-order ordinary differential equation for $\gamma(\xi)$, or as one of a pair of first-order coupled ordinary differential equations determining $\gamma(\xi)$ and $\pi(\xi)$, the other equation being simply

$$\gamma'(\xi) = \pi(\xi). \tag{23}$$

This second interpretation is the one we adopted in [4] and [5], and we will also adopt it here. This pair of first-order ordinary differential equations can be used for the numerical integration of this differential system, in order to obtain $\gamma(\xi)$ and $\beta(r)$, as we in fact did in those papers, and as we will do here as well. It is important to note that in terms of these dimensionless variables the equation of state shown in Equation (8) can be written as

$$\bar{P}(\xi) = C \left[\bar{\rho}(\xi)\right]^{1+1/n}, \tag{24}$$

where we define the dimensionless pressure and energy density by

$$\bar{P}(\xi) = \kappa r_0^2 P(\xi), \tag{25}$$

$$\bar{\rho}(\xi) = \kappa r_0^2 \rho(\xi). \tag{26}$$

We also have for the relation in Equation (7), when written in terms of the dimensionless variables,

$$\pi(\xi) = \xi^2 \bar{\rho}(\xi). \tag{27}$$

Note that in this formulation of the problem all dimensionfull physical quantities have vanished from view, so that the problem is reduced to purely mathematical terms. All that is involved is a dimensionless function $\gamma(\xi)$ of a dimensionless variable ξ, its derivative $\pi(\xi)$, and two dimensionless positive real constants, n and C. In particular, the mass M and the Schwarzschild radius r_M no longer appear explicitly in the equations. In essence they have been replaced by the parameters r_0, that does not appear explicitly at all, and ξ_M, that appears only as the asymptotic limit of $\gamma(\xi)$. The mass M is a free parameter of the system that has effectively been factored out of it.

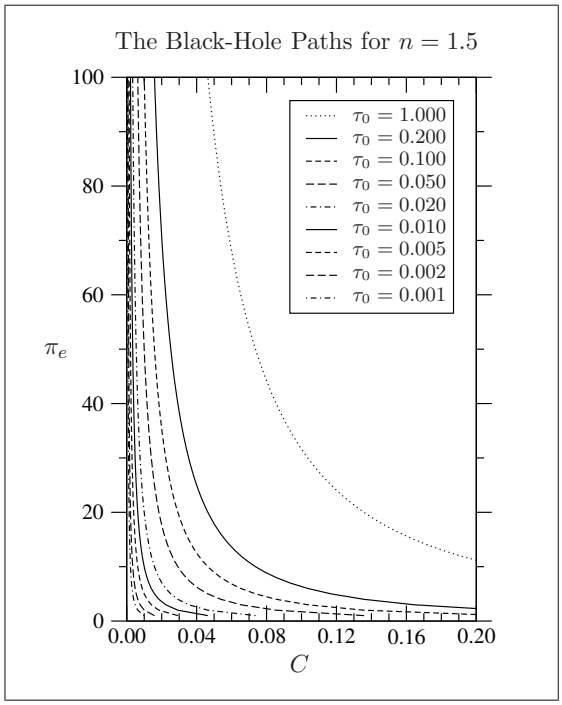

Figure 1: Left: Case $n = 1.5$.

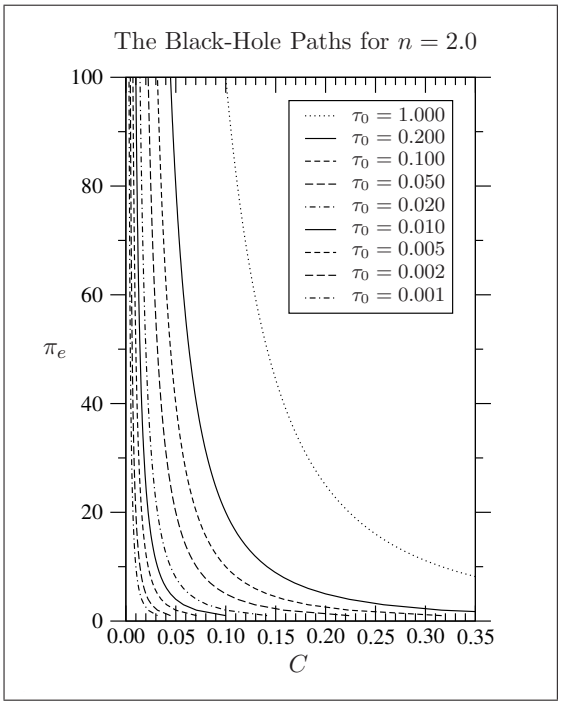

Figure 2: Right: Case $n = 2.0$.

Figures 1–2: The paths used for the black-hole limits, within the (C, π_e) parameter planes. The dotted curves, that correspond to $\tau_0 = 1$, are the asymptotes to the DEC curves.

3 Description of the Exploration

Let us start by recalling the properties of the allowed regions within the (C, π_e) parameter planes. For each value of n the allowed region is limited by the π_e axis and by two curves in the corresponding (C, π_e) parameter plane, as can be seen in the graphs presented in [5]. Below, for the smaller values of π_e, we have the Tooper curve, and above, for the larger values of π_e, we have the DEC (Dominant Energy Condition) curve. The Tooper curve starts at the origin $(C, \pi_e) = (0, 0)$ and has positive derivative everywhere. The DEC curve diverges to $\pi_e \to \infty$ near $C = 0$ and has negative derivative everywhere. These two curves eventually cross at some finite value of C, which is therefore the maximum possible value of C for that value of n. All existing and physically acceptable solutions must be above the Tooper curve, below that DEC curve, and away from the π_e axis, where there are no stable solutions. The DEC curve is always somewhat below the asymptote given by the simple relation

$$\pi_e(C) = \frac{1}{C^n}, \tag{28}$$

and becomes progressively closer to that asymptote as π_e increases. Therefore, when we make $\pi_e \to \infty$ it is necessary to also make $C \to 0$, in order to stay within the allowed region, below the DEC curve. For each value of n what we refer to as the "asymptotic region" is the portion of the allowed region for very large values of π_e and hence for very small but non-zero values of C.

Our first question here is that of deciding how to scan this region in the best possible

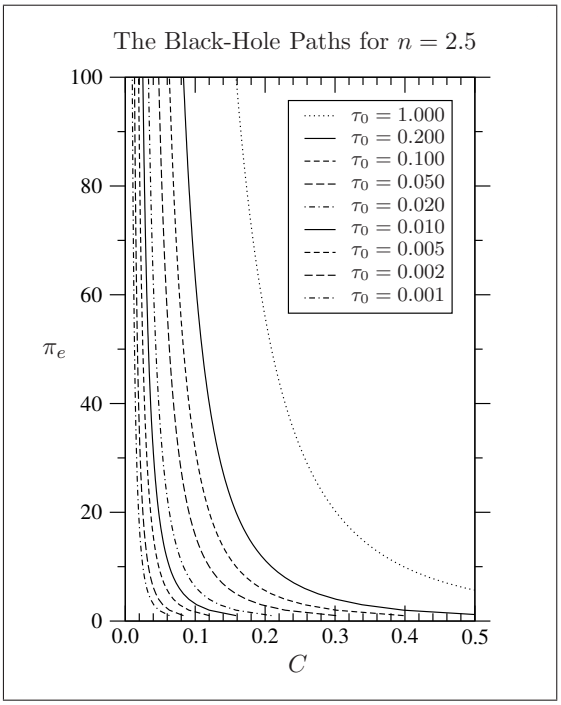

Figure 3: Left: Case $n = 2.5$.

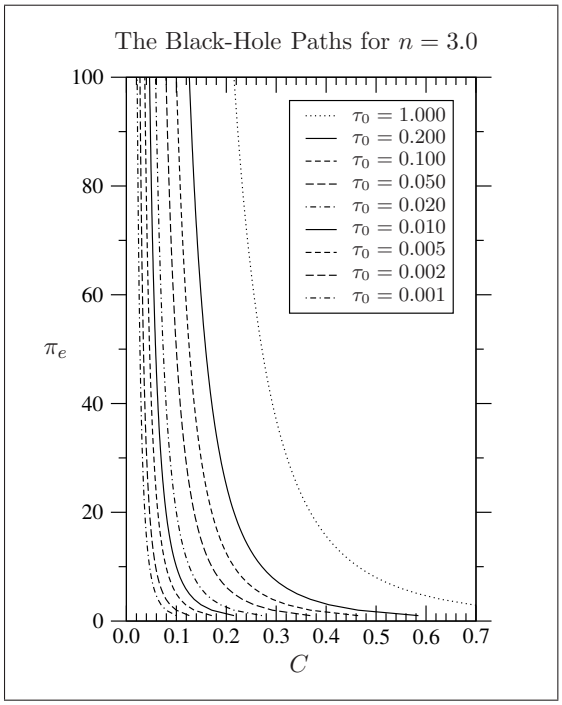

Figure 4: Right: Case $n = 3.0$.

Figures 3–4: The paths used for the black-hole limits, within the (C, π_e) parameter planes. The dotted curves, that correspond to $\tau_0 = 1$, are the asymptotes to the DEC curves.

way. In order to do this we will define a family of curves along which one can take limits that go indefinitely deep into this asymptotic region. These paths for the limits are proportional do the asymptote, being a certain factor $\tau_0 < 1$ below it, and are given by

$$\pi_e(C) = \tau_0 \, \frac{1}{C^n}. \tag{29}$$

The larger τ_0 becomes, up to the position of the DEC curve, the closer the path is to that curve, near which the matter displays deep relativistic behavior, with extremely high temperature and very large speed of sound, close to c. The smaller τ_0 is, the closer we get to the low-temperature, low thermal speed regime. Note that τ_0 is essentially a measure of the local temperature of the matter. In the graphs shown in Figures 1 through 4 we can see these curves within the (C, π_e) parameter planes for the four particular values of n used in this paper, and a set of 8 values of τ_0 over a fairly wide range. The values used for n are 1.5, 2.0, 2.5 and 3.0. The values used for τ_0 are 0.001, 0.002, 0.005, 0.01, 0.02, 0.05, 0.1 and 0.2. The value $\tau_0 = 1$ corresponds, of course, to the asymptote itself, and is used here only as a visual reference.

In the graphs shown in Figures 5 through 8 we can see a visual representation of the black hole limits, for limits along paths in the parameter planes such as those described in Equation (29), for $n = 1.5$, from the point of view of the central function $\gamma(\xi)$ of the family of exact solutions. In obtaining these graphs we used for the parameter r_0 the position r_e of the inflection point of $\beta(r)$, so that we have for the corresponding dimensionless radial position $\xi_e = r_e/r_0$ of the inflection point of $\gamma(\xi)$ the value $\xi_e = 1$. In fact, the same choice was used in all the runs involved in the results shown in this paper. These graphs show

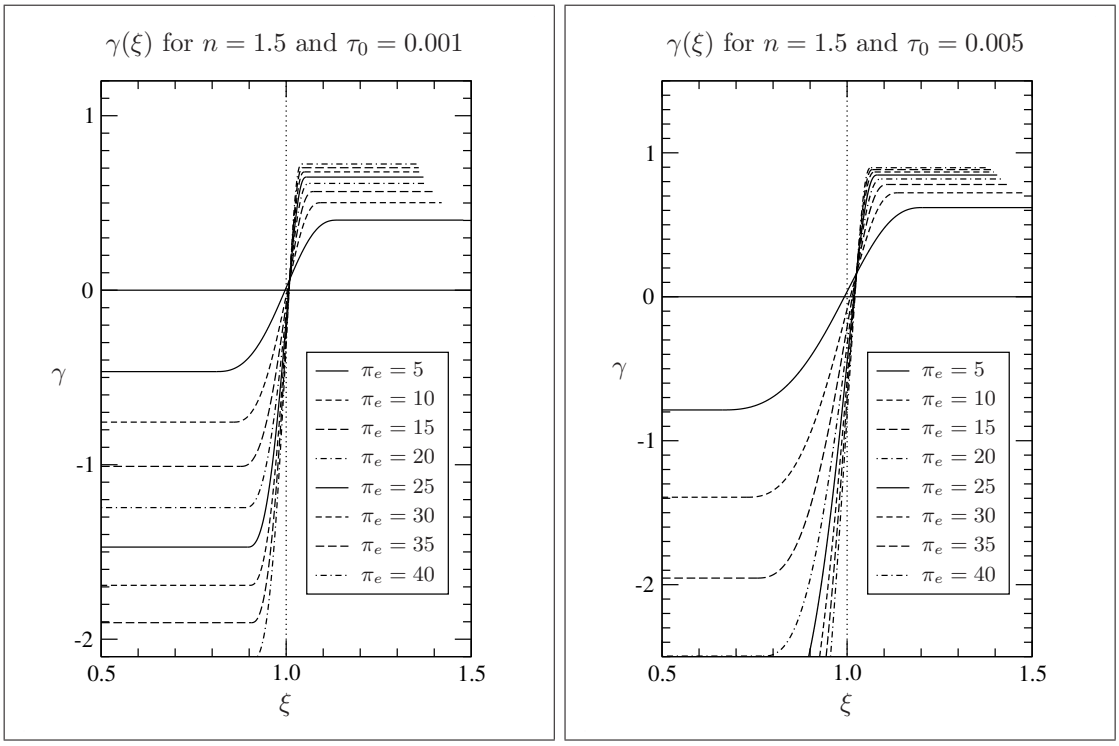

Figure 5: Left: Case $\tau_0 = 0.001$.

Figure 6: Right: Case $\tau_0 = 0.005$.

Figures 5–6: Sequences of functions $\gamma(\xi)$ for $n = 1.5$ and for a sequence of values of π_e from 5 to 40, illustrating the approach to a black-hole configuration.

sequences of functions $\gamma(\xi)$ obtained numerically for a corresponding sequence of 8 values of π_e, representing the starting part of a black-hole limit, namely the values 5, 10, 15, 20, 25, 30, 35 and 40. The dotted vertical line at $\xi = 1$ is the starting point of the numerical integration to either side, and is the common inflection point of all the curves shown. This is also the common point of maximum of the derivatives $\pi(\xi)$ of $\gamma(\xi)$.

The constant values of $\gamma(\xi)$ to the left correspond to the inner vacuum region, and the constant values to the right correspond to the outer vacuum region. The constant values to the left diverge to $-\infty$ in the black-hole limits, and those to the right accumulate towards a finite value of the order of 1. Since the constant values to the left are given by $-\xi_\mu$, this divergence on the left corresponds to the divergence of ξ_μ and r_μ to infinity, and since the constant values to the right are given by ξ_M, they thus correspond to finite values of r_M in the black-hole limits. One can see that in the black-hole limits the function $\gamma(\xi)$ approaches a point of non-differentiability at the position r_2 of the outer surface of the matter. This indicates the formation of the event horizon.

Our next task at this point is to determine how the parameter ξ_μ behaves along these curves. This can be seen on the graphs shown in Figure 9, for the value of $n = 1.5$, and for π_e varying from 1 to 500. In Appendix A one can find a more complete set of graphs, for all the values of n used. The behavior of $\xi_\mu(\pi_e)$ in all cases is similar to the one seen in Figure 9. As can be seen in that graph, ξ_μ is essentially linear with π_e, specially for the larger values of π_e. We included in these graphs linear fits for ξ_μ, calculated for the 100 larger values of π_e, given by

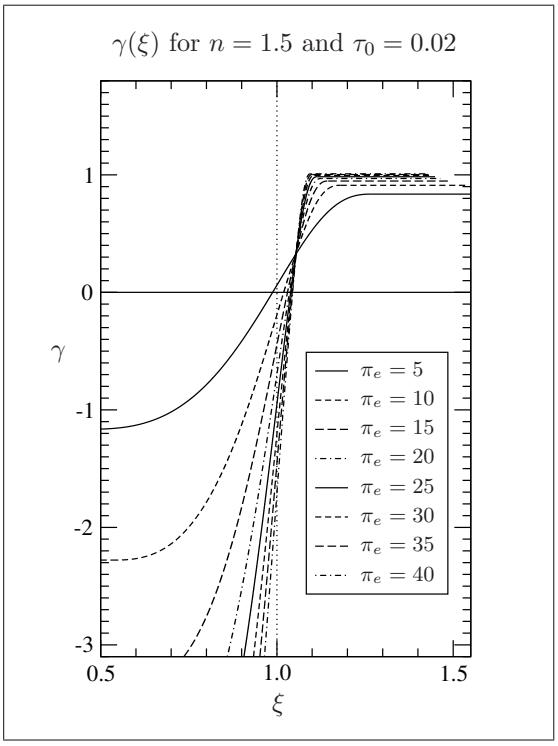

Figure 7: Left: Case $\tau_0 = 0.02$.

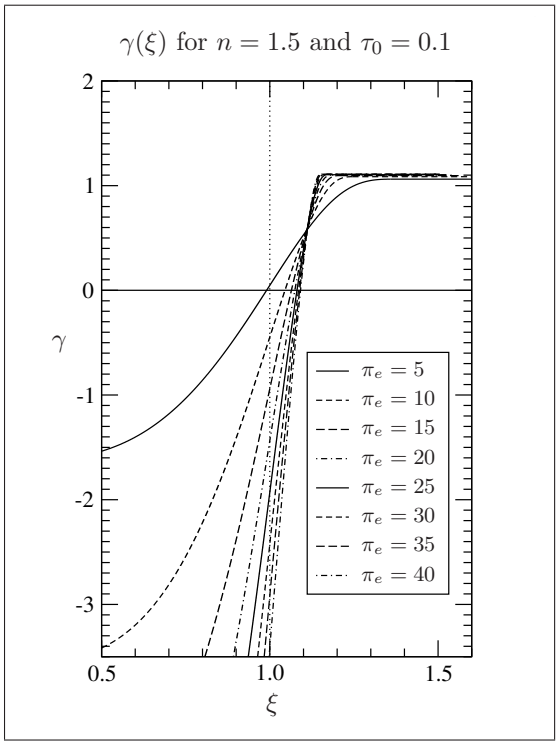

Figure 8: Right: Case $\tau_0 = 0.1$.

Figures 7–8: Sequences of functions $\gamma(\xi)$ for $n = 1.5$ and for a sequence of values of π_e from 5 to 40, illustrating the approach to a black-hole configuration.

$$\xi_\mu(\pi_e) = \alpha_0 + \alpha_1 \pi_e. \tag{30}$$

These fits turn out to be essentially exact within the numerical precision used. The regression correlation coefficients are consistently equal to 1 within that numerical precision. The errors in the coefficients are negligible. Table 1 shows the linear regression coefficients α_0 and α_1 shown in Equation (30), for all values of n used. The regressions are applied in each case to the last 100 of the 500 values of π_e used, that is, from $\pi_e = 401$ to $\pi_e = 500$. This shows that for large values of π_e the dimensionless radius ξ_μ is very precisely linear with π_e, with fairly small deviations only for very small values of π_e.

The following important conclusion can be drawn from this analysis. Since the black-hole limits are obtained when we make $\pi_e \to \infty$, it follows that we always have that

$$\xi_\mu \to \infty, \tag{31}$$

in all black-hole limits. This means that the $\xi_\mu \to \infty$ limit is equivalent to the $\pi_e \to \infty$ limit, as a way to characterize the black-hole limits. This implies, in particular, that in such limits r_μ always diverges to infinity, as does the energy μc^2 associated to it.

The exploration of the black-hole limits was performed in terms of certain useful diagnostic variables. These diagnostic observable are the same that were previously defined and used in [5], namely the ratios

$$E_R \;=\; \frac{r_\mu}{r_M + r_\mu}$$

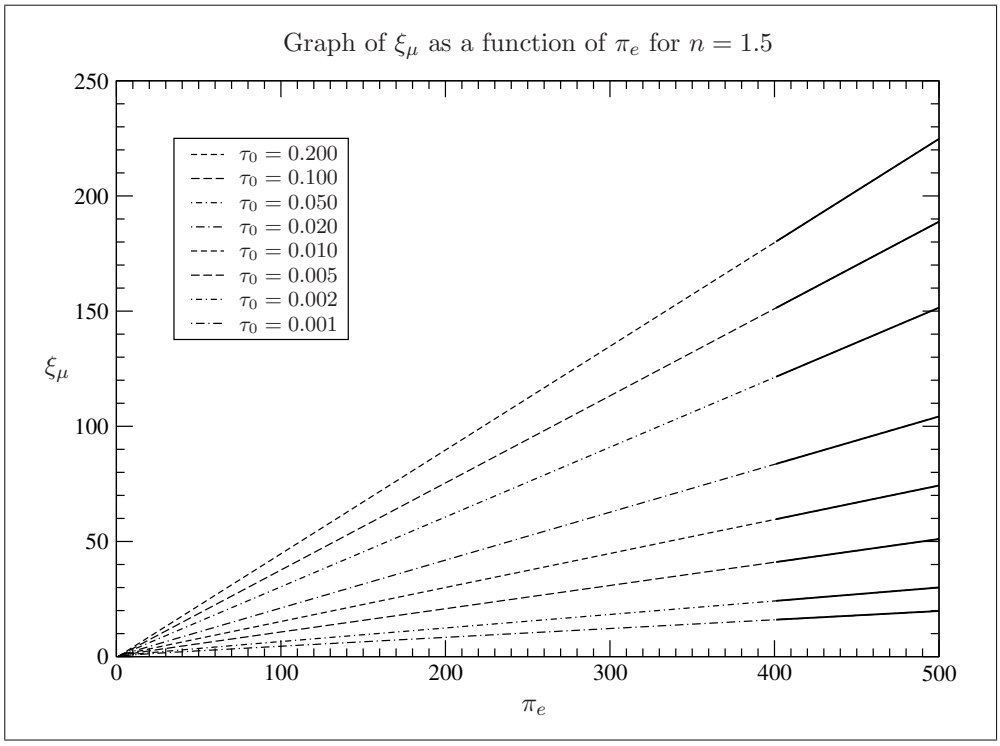

Figure 9: The behavior of ξ_μ as a function of π_e for the case $n = 1.5$, for the eight values of τ_0 used. The heavy solid lines are linear fits to the last 100 point of each graph, which turn out to be perfect fits within the numerical precision used. A more complete set of graphs, for all values of n, can be found in Appendix A.

$$= \frac{\xi_\mu}{\xi_M + \xi_\mu}, \tag{32}$$

$$H_R = \frac{r_M}{r_2}$$

$$= \frac{\xi_M}{\xi_2}, \tag{33}$$

$$Q_R = \frac{r_1}{r_2}$$

$$= \frac{\xi_1}{\xi_2}, \tag{34}$$

all of which assume values within the interval $[0, 1]$. The first one, in Equation (32), we refer to as the Energy Ratio, the second one, in Equation (33), as the Horizon Ratio, and the last one, in Equation (34), as the Quantum Ratio. The meanings of these observables were discussed in [5], and we will quickly review them here.

The Energy Ratio E_R has the property of being equal to zero at the Tooper curve and, since we just saw that $\xi_\mu \to \infty$ in the black-hole limits, it has the property of tending to 1 in such limits. It therefore distinguishes and interpolates between the Tooper solutions and the black-hole limits. The Horizon Ratio H_R, by comparing the Schwarzschild radius r_M with the outer radius r_2, characterizes the overall energy density of the solution, as well as the proximity to the formation of an event horizon at r_2. It is very small for the very low-density solutions, and tends to 1 in the black-hole limits.

The Quantum Ratio Q_R, by comparing the inner radius r_1 with the outer radius r_2,

n	τ_0	α_0	α_1	n	τ_0	α_0	α_1
1.5	0.200	−0.3852892	0.4503448	2.5	0.200	−0.4782566	0.5275016
	0.100	−0.1936474	0.3780476		0.100	−0.3971084	0.4800606
	0.050	+0.0359390	0.3029430		0.050	−0.3002054	0.4337708
	0.020	+0.3386680	0.2078438		0.020	−0.1490952	0.3726328
	0.010	+0.5254569	0.1475215		0.010	−0.0214393	0.3262976
	0.005	+0.6608857	0.1007877		0.005	+0.1115560	0.2806850
	0.002	+0.7646767	0.0585121		0.002	+0.2838054	0.2235925
	0.001	+0.7949933	0.0380426		0.001	+0.4032393	0.1844273
2.0	0.200	−0.4488262	0.4964475	3.0	0.200	−0.4948009	0.5502534
	0.100	−0.3329712	0.4403132		0.100	−0.4328028	0.5085879
	0.050	−0.1912202	0.3839310		0.050	−0.3605405	0.4685270
	0.020	+0.0257299	0.3083408		0.020	−0.2490029	0.4165601
	0.010	+0.1962239	0.2525214		0.010	−0.1534554	0.3774229
	0.005	+0.3563128	0.2008355		0.005	−0.0503161	0.3384133
	0.002	+0.5341043	0.1425684		0.002	+0.0926441	0.2876908
	0.001	+0.6368277	0.1073342		0.001	+0.2010366	0.2507694

Table 1: The linear regression coefficients for the graphs in Figure 9, as well as in Figures A01–A04 of Appendix A. The coefficient α_0 is the intercept and the coefficient α_1 is the slope. The errors in the coefficients, and specially in the slope, are negligible.

identifies situation in which the quantum properties of matter come into play. It is zero at the Tooper solutions, which are characterized by having $r_1 = 0$, as well as by having $r_\mu = 0$, and tends to 1 when the width of the matter shell tends to zero. In such situations, when the proper width of the matter shell approaches the wavelength of the fields associated to the particles of matter contained within it, the quantum behavior of that matter will prevent the shell from becoming any thinner. It would therefore be physically impossible to actually take a physical limit in which Q_R assumes the value 1.

4 Results of the Exploration

The behavior of the diagnostic observables along the paths shown in Figures 1 through 4 can be seen in Figures 10 through 12. The values used for π_e were the integers, starting from 1 and going up to 500. For each one of the graphs shown here, which are all for the case $n = 1.5$, more complete sets of graphs, for all values of n that were used, can be found in Appendix A. In the numerical runs used to obtain all these graphs we used for the parameter r_0 the position r_e of the inflection point of $\beta(r)$, so that we have for the corresponding dimensionless radial position $\xi_e = r_e/r_0$ of the inflection point of $\gamma(\xi)$ the value $\xi_e = 1$.

4.1 Behavior of the Limits

The graphs of $E_R(\pi_e)$ shown in Figure 10 indicate that in all these limits we have that $E_R(\pi_e) \to 1_\ominus$, which corresponds to $\xi_\mu \to \infty$, as we already know must be the case. This shows quite clearly that all these limits are in fact black-hole limits, in the sense that ξ_μ diverges on them. The pace of the approach of E_R to 1 varies with the parameter τ_0. It is somewhat slower for the low-temperature cases, with smaller values of τ_0, and faster for the

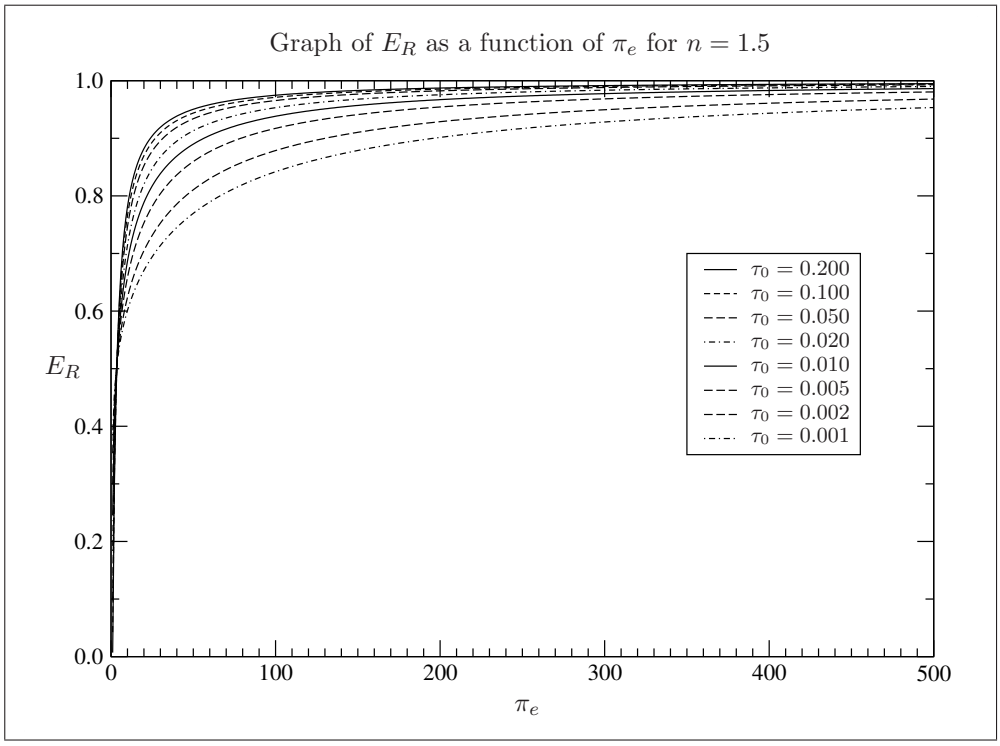

Figure 10: The behavior of E_R as a function of π_e for the case $n = 1.5$, for the eight values of τ_0 used. A more complete set of graphs, for all values of n, can be found in Appendix A.

high-temperature cases, with larger values of τ_0. The conclusion here is that the black-hole limits seem to exist and to behave, by and large, as expected.

The graphs of $H_R(\pi_e)$ shown in Figure 11 indicate that in all these limits we have that $H_R(\pi_e) \to 1_\ominus$ as well, which corresponds to $\xi_M \to \xi_{2\ominus}$. Once more, this shows quite clearly that all these limits are in fact black-hole limits, in the sense that they approach the formation of an event horizon at the position r_2 of the outer surface of the matter. Once again, the pace of the approach of H_R to 1 varies with the parameter τ_0. It is somewhat slower for the low-temperature cases, with smaller values of τ_0, and faster for the high-temperature cases, with larger values of τ_0. The conclusion here is that these limits do indeed take us to black-hole solutions, that display an event horizon at r_2. In the limit the exterior part of the solution is indistinguishable from the solution for a naked black hole, represented by the exterior Schwarzschild solution for all $r > r_2$.

In the case of the graphs of $Q_R(\pi_e)$ shown in Figure 12, on the other hand, we see a very different picture. The graphs of $Q_R(\pi_e)$ indicate that for each value of τ_0 this observable approaches a constant value smaller than 1, as we make $\pi_e \to \infty$, with values that depend on τ_0. We must therefore conclude that in the limits along the paths shown in Figures 1 through 4 the observable $Q_R(\pi_e)$ does *not* tend to 1 when we make $\pi_e \to \infty$. Instead, it tends to constant values that are strictly smaller than 1. For the larger values of τ_0 they are significantly smaller than one, and for the smaller values of τ_0 they are close to 1. However, they do not tend to 1 in the limit, so that the coordinate thickness $r_2 - r_1$ of the matter shell does *not* tend to zero. Therefore in these limits we always have that $r_1 < r_2$. The conclusion here is that there are different types of such black-hole limits, in which the local temperature of the matter has different values. Since τ_0 varies monotonically with the local temperature of the matter, for large values of τ_0 the temperature will be large,

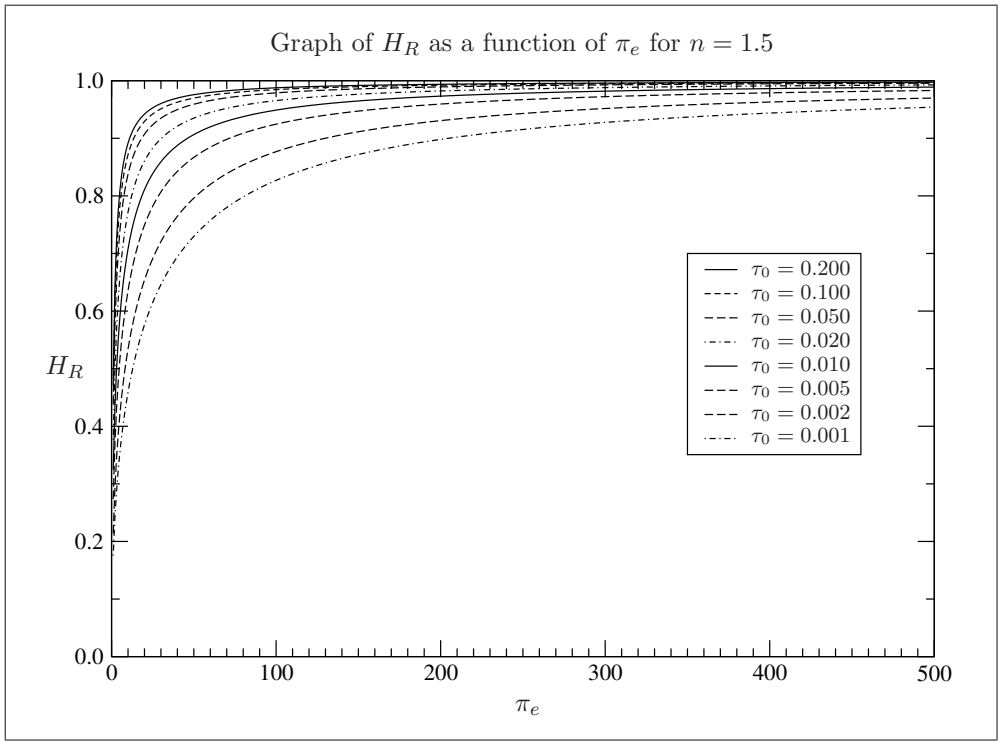

Figure 11: The behavior of H_R as a function of π_e for the case $n = 1.5$, for the eight values of τ_0 used. A more complete set of graphs, for all values of n, can be found in Appendix A.

and for small values of τ_0 the temperature will be small. Only for very low temperatures the proper thickness of the matter shell will be commensurate with the wavelength of the matter fields, so that the quantum limitations on the behavior of matter come into play.

One can verify that in the cases of $E_R(\pi_e)$ and $H_R(\pi_e)$ the functions do tend to 1, and that they do so with a power behavior, by making logarithmic plots of the quantities $1 - E_R(\pi_e)$ and $1 - H_R(\pi_e)$. The graphs of $\ln(1 - E_R)$ and $\ln(1 - H_R)$ versus $\ln(\pi_e)$ are shown in Figures 13 and 14. The curves tend to behave as straight lines for large values of π_e, which indicates that $[1 - E_R(\pi_e)]$ and $[1 - H_R(\pi_e)]$ decrease asymptotically to zero as powers. The absolute value of the negative slopes of the graphs are smaller than and close to 1, indicating that these quantities fall to zero approximately as $1/\pi_e$.

Due to the behavior of $Q_R(\pi_e)$ in these limits, so far we must conclude that all these limits correspond to non-zero local matter temperatures. In order to construct a limit in which the local matter temperature tends to zero, we must decrease C faster than in the limits that we have been using so far, given in Equation (29) or, in other words, we must increase π_e slower as $C \to 0$. This can be accomplished with limits along paths given by

$$\begin{aligned} \pi_e(C) &= \tau_0 \frac{1}{C^{n-\varepsilon}} \\ &= \tau(C) \frac{1}{C^n}, \end{aligned} \tag{35}$$

where $\varepsilon > 0$, which corresponds to a decreasing temperature as $C \to 0$, and where $\tau(C)$ is given by

$$\tau(C) = \tau_0 C^{\varepsilon}. \tag{36}$$

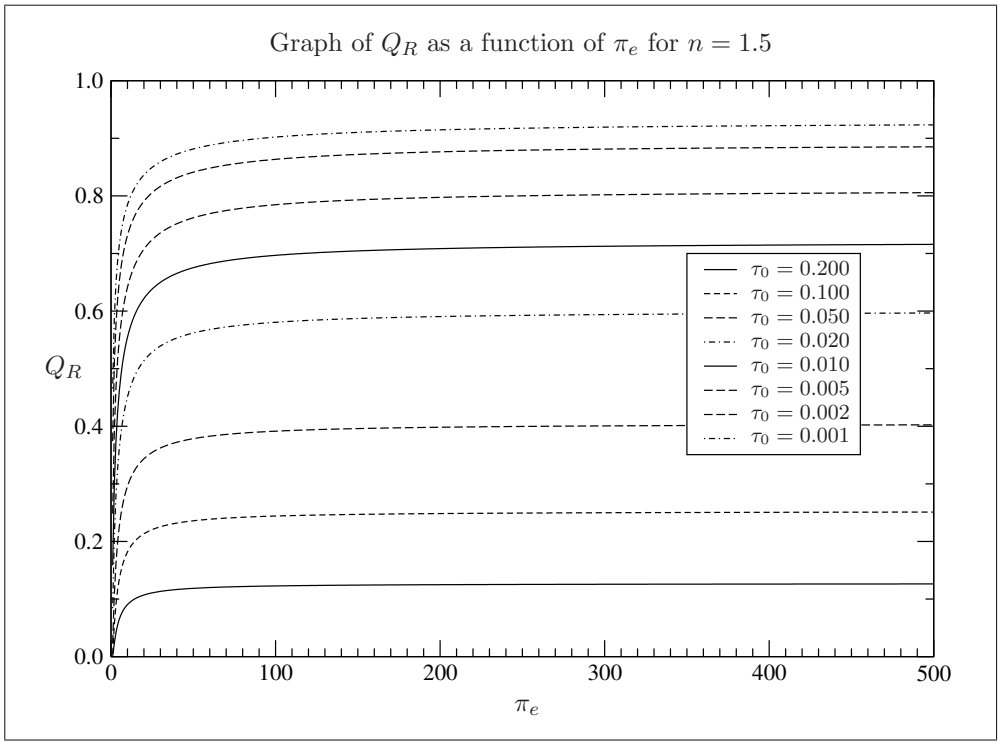

Figure 12: The behavior of Q_R as a function of π_e for the case $n = 1.5$, for the eight values of τ_0 used. A more complete set of graphs, for all values of n, can be found in Appendix A.

One can see the behavior of $Q_R(\pi_e)$ in these new limits in Figure 15, for the case $\varepsilon = 0.5$. In this new type of limit we have that $Q_R \to 1$ when $\pi_e \to \infty$. For the smaller values of τ_0, and therefore the smaller decreasing temperatures, the approach of Q_R to 1 is faster, and for the larger values of τ_0, and therefore the larges decreasing temperatures, the approach of Q_R to 1 is slower. But in any case we will always end up with $Q_R = 1$ in the limit, which means that in these limits we will always approach the limitations associated to the quantum behavior of the matter, for any value of τ_0. As is to be generally expected, the quantum effects appear predominantly when the matter is at low temperatures. One can see in Figure 16 the graphs of $\ln(1 - Q_R)$ versus $\ln(\pi_e)$ in this new type of limit. Once more the curves tend to behave as straight lines for large values of π_e, which indicates that $[1 - Q_R(\pi_e)]$ decreases to zero as a power.

In the new type of limit just discussed, we have that $\pi_e(C)$ diverges to infinity slower than $1/C^n$, as we make $C \to 0$, since we have that $\varepsilon > 0$. One might also consider limits in which $\pi_e(C)$ diverged to infinity faster that $1/C^n$, which would correspond to $\varepsilon < 0$. However, in this case $\pi_e(C)$ would increase faster than the asymptote of the DEC curve, and would therefore eventually cross the DEC curve, so that the solutions would become incompatible with the Dominant Energy Condition. Therefore these are not useful limits.

4.2 Feasibility of the Limits

We must now discuss whether or not these black-hole limits can actually be taken, from the physical standpoint. We will see that there are at least three issues involved, leading to the conclusion that the black-hole limits cannot actually be physically taken. The first is a question of mathematical consistency. Since the paths of the black-hole limits in the parameter planes are below the curve $\pi_e = 1/C^n$, and since during the limit we necessarily

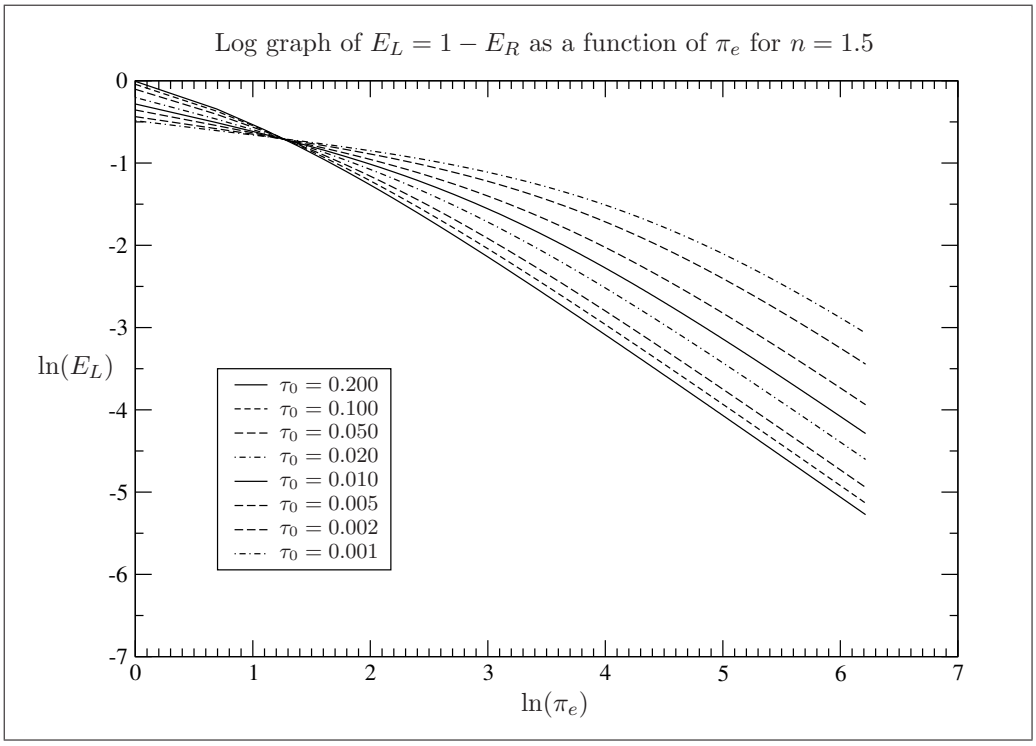

Figure 13: Logarithmic plot of the behavior of $1 - E_R$ as a function of π_e for the case $n = 1.5$, for the eight values of τ_0 used. A more complete set of graphs, for all values of n, can be found in Appendix A.

have that $\pi_e \to \infty$, it follows that we must also have $C \to 0$. However, according to Equation (24) the value $C = 0$ corresponds to pressureless dust, and hence for this value of C there can be no static solution, thus leading to a mathematical inconsistency.

The second issue comes from the fact that, since we saw that in the $\pi_e \to \infty$ black-hole limits we have that $\xi_\mu \to \infty$, it follows that we also have that $r_\mu \to \infty$ and $\mu c^2 \to \infty$, where $\mu c^2 = r_\mu c^4/(2G)$. The quantity μc^2 is an energy, that as we will see shortly can be written in terms of the matter energy density, whose complete nature may not yet be entirely clear, but that can be associated to some combination of the thermal energy of the system and the gravitational binding energy of the system. Having this energy diverge to infinity would mean that some of these forms of energy diverge to infinity, which is physically impossible.

The third issue comes from the fact that, as we saw, the black-hole limits in which the local matter temperature goes to zero have the property that the quantum ratio behaves as $Q_R \to 1$. These zero-temperature limits take us to a situation where the quantum properties of the matter prevent us from further compressing the matter, and hence force the process of taking the limits to be halted. Even if this process is rather slow, and allows the limit to proceed to an extraordinary extent, it still stops us from being able to assign any real physical significance to the limit itself.

In order to further examine the last two issues, we can construct an interesting integral involving energies and the matter energy density. Using Equation (13), and integrating over a spherically symmetric coordinate volume from the position r_z of the zero of $\beta(r)$ to the outer radius r_2, we get

$$4\pi \int_{r_z}^{r_2} dr\, r^2 \rho(r) = 4\pi \, \frac{r_M}{\kappa} \int_{r_z}^{r_2} dr\, \beta'(r). \tag{37}$$

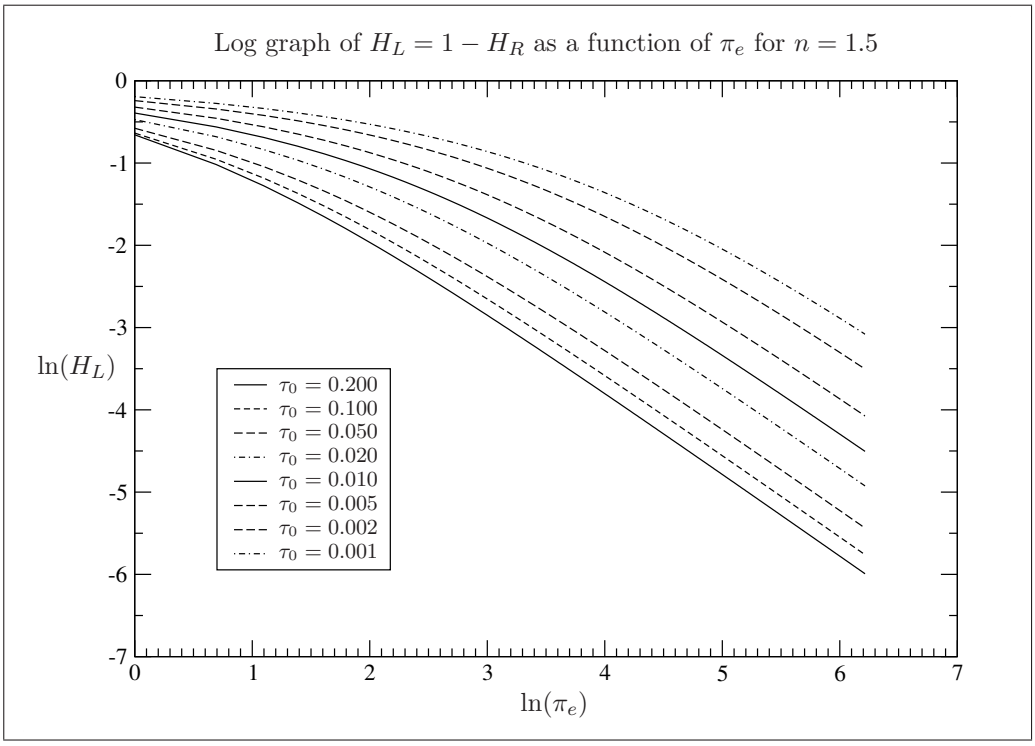

Figure 14: Logarithmic plot of the behavior of $1 - H_R$ as a function of π_e for the case $n = 1.5$, for the eight values of τ_0 used. A more complete set of graphs, for all values of n, can be found in Appendix A.

One can now see that the integral on the right-hand side is trivial, and since we have that $\beta(r_z) = 0$ and that $\beta(r_2) = 1$, we get

$$Mc^2 = 4\pi \int_{r_z}^{r_2} dr\, r^2 \rho(r), \tag{38}$$

where we have replaced κ and r_M by their values in terms of M, G and c. We have therefore an expression for the physically meaningful energy Mc^2 in terms of a coordinate volume integral of the matter energy density. Note however that the integral does not run over the whole matter region, since it starts at $r_z > r_1$ rather than at r_1. Therefore, if we consider the integral from r_1 to r_z, in a similar way we get

$$4\pi \int_{r_1}^{r_z} dr\, r^2 \rho(r) = 4\pi \frac{r_M}{\kappa} \int_{r_1}^{r_z} dr\, \beta'(r). \tag{39}$$

Once again one can see that the integral on the right-hand side is trivial, and since we have that $\beta(r_z) = 0$ and that $\beta(r_1) = -r_\mu / r_M$, we now get

$$\mu c^2 = 4\pi \int_{r_1}^{r_z} dr\, r^2 \rho(r), \tag{40}$$

where we have now replaced κ and r_μ by their values in terms of μ, G and c. We have therefore an expression for the energy μc^2 in terms of another coordinate volume integral of that same energy density, this time over the remaining part of the matter region. It is at least a reasonable assumption that this energy must be physically meaningful, just like the energy Mc^2, even if its complete physical meaning is not entirely clear yet.

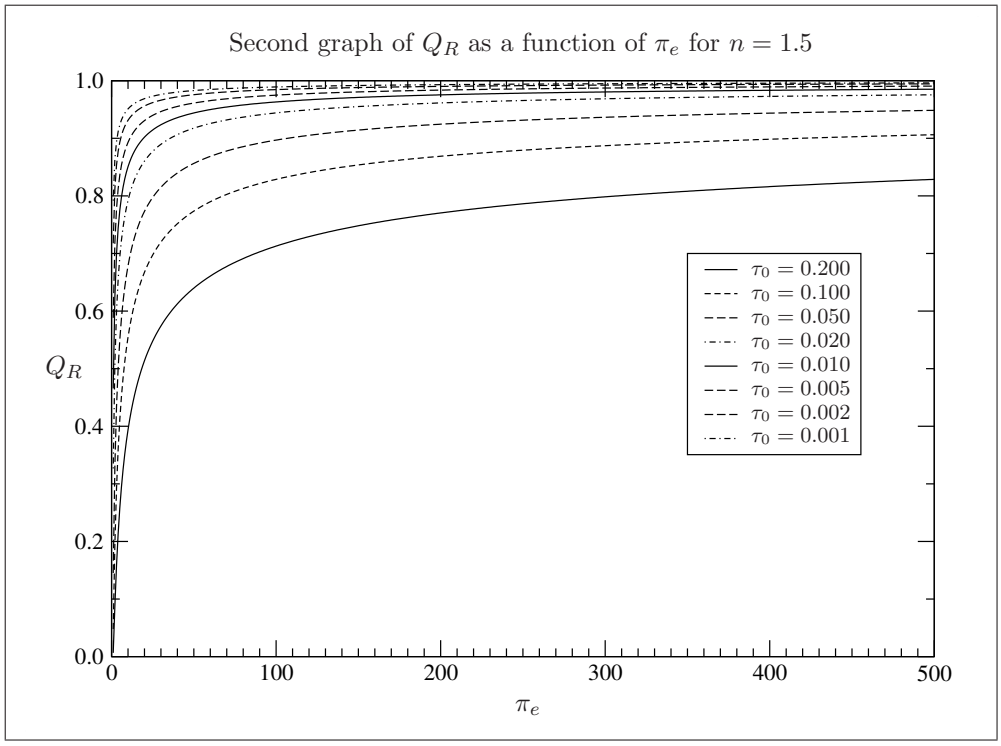

Figure 15: The behavior of Q_R as a function of π_e for the case $n = 1.5$, for the eight values of τ_0 used, in the case of the second type of limit, with $\varepsilon = 0.5$. A more complete set of graphs, for all values of n, can be found in Appendix A.

If we now consider the integral over the whole matter region, due to the additive property of the integrals over the union of disjoint domains, using Equations (38) and (40) we obtain the result that

$$4\pi \int_{r_1}^{r_2} dr\, r^2 \rho(r) = \mu c^2 + Mc^2. \tag{41}$$

Now, in the black-hole limit we have that $r_\mu \to \infty$, which implies that $\mu \to \infty$. Since M is finite and the integration domain is a finite interval, this implies that the integrand has to diverge in order for the integral do diverge to infinity, and since r is within that finite interval, it is necessary that $\rho(r) \to \infty$ within some interval with non-zero length, and in particular that its maximum value, which is necessarily assumed somewhere within the interval, diverges. In addition to this, it follows that this divergence of $\rho(r)$ is a non-integrable one. Therefore, so long as $r_2 - r_1$ does not go to zero, the black-hole limit implies the existence of infinite concentrations of matter, resulting in infinite energies, since μc^2 goes to infinity, a situation which is physically unacceptable.

The only possible alternative to the situation just described is that we have a black-hole limit in which $r_2 - r_1 \to 0$ in the limit, in which case we now have that $Q_R(\pi_e) \to 1$, and hence we have in force the limitation that eventually the quantum properties of matter will prevent us from taking the limit to its ultimate conclusion. We see, therefore, that in either case the black-hole limit cannot really be taken in a physically meaningful way.

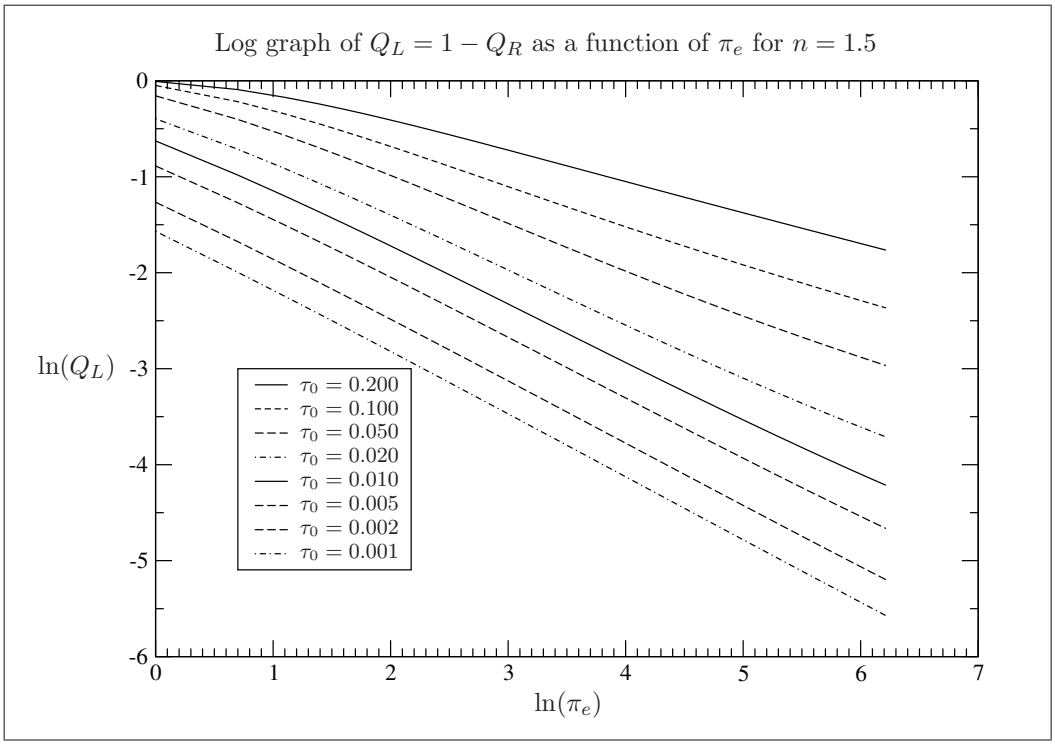

Figure 16: Logarithmic plot of the behavior of $1 - Q_R$ as a function of π_e for the case $n = 1.5$, for the eight values of τ_0 used, in the case of the second type of limit, with $\varepsilon = 0.5$. A more complete set of graphs, for all values of n, can be found in Appendix A.

5 Analysis of the Interior Geometry

Let us now inquire into the nature of the spacetime geometry of the interior region in the black-hole limits. The spatial geometry is given by the radial and angular proper lengths between pairs of points. By symmetry we may limit the discussion to the plane $\theta = \pi/2$. In this case the elements of proper arc-lengths along the angle ϕ are simply given by $d\ell_\phi = r\, d\phi$, and the elements of proper radial distance are given by $d\ell_r = \exp[\lambda(r)]\, dr$. Inside the inner vacuum this is given by

$$d\ell_r = \sqrt{\frac{r}{r + r_\mu}}\, dr, \tag{42}$$

$$d\ell_\phi = r\, d\phi, \tag{43}$$

and integrating between two given points in either case we get the proper lengths

$$\ell_r = \int_{r_a}^{r_b} dr \sqrt{\frac{r}{r + r_\mu}}, \tag{44}$$

$$\ell_\phi = r(\phi_b - \phi_a). \tag{45}$$

While in the $\pi_e \to \infty$ black-hole limits ℓ_ϕ does not change at all, in the case of ℓ_r, since in the $\pi_e \to \infty$ limits we have that $r_\mu \to \infty$, it follows that

$$\lim_{\pi_e \to \infty} \ell_r = \lim_{r_\mu \to \infty} \int_{r_a}^{r_b} dr \sqrt{\frac{r}{r + r_\mu}}. \tag{46}$$

This is the integral of a limited function over a finite interval, and is therefore finite. Since in the limit the denominator of the integrand increases without bound, it follows that

$$\lim_{\pi_e \to \infty} \ell_r = 0, \tag{47}$$

for all values of r_a and r_b, of any two points aligned along a radius, within the inner vacuum region $[0, r_1]$. In fact, it can be verified numerically that, since within the matter region we have that, from Equation (5),

$$\mathrm{e}^{\lambda(r)} = \sqrt{\frac{r}{r - r_M \beta(r)}}, \tag{48}$$

where everywhere strictly to the left of its single zero at r_z the function $\beta(r)$ is negative and tends to $-\infty$ in the black-hole limits, this result can actually be extended to the part of the matter region that is strictly to the left of the single zero of $\beta(r)$. The conclusion is that in this whole inner region, from $r = 0$ to the zero r_z of $\beta(r)$, given any two points r_a and r_b along the radial direction, the distance between them goes to zero in the black-hole limits. It follows, in particular, that the whole actual proper width of the matter region in the black-hole limits lies entirely within the interval $[r_z, r_2]$.

If we now consider the distance between any two points within this inner region $[0, r_z]$, for any values of the angles, to be the minimum possible path length among all the possible paths connecting the two points, then this implies that the distance between *any* two points within this region goes to zero in the black-hole limits. This is so because we can always first go to the center along a radial direction, and then go out again to the other point along another radial direction. Both legs of this path have length zero in the limit, and therefore the overall distance is zero. Therefore, all the distances between pairs of points within the inner region $[0, r_z]$ collapse to zero in the black-hole limits.

This implies that any events occurring at these points, such as, for example, thermal of quantum fluctuations, will be completely correlated to one another. The same is true for any two points located outside the inner region but sufficiently close to r_z. All the points within the inner region will in fact act as a single point, notwithstanding the fact that there are paths with non-zero lengths connecting pairs of such points, such as angular paths. The minimum length of all possible paths connecting any two points is always zero. In black-hole limits in which r_1 approaches r_2, typically in the zero-temperature cases, this behavior will extend to the whole interior of the black hole, inside the event horizon. It is to be presumed that this is the case for what are usually called "naked black hole" solutions, with no matter at all at or outside the horizon. In this case we see that all the points of the horizon are fully correlated to one another.

In the way of confirmation of these results, it is interesting to note that the integral in Equation (46) can be calculated exactly. Using the dimensionless variables and parameters $\chi = r/r_\mu$, $\chi_a = r_a/r_\mu$ and $\chi_b = r_b/r_\mu$, leading to $d\chi = dr/r_\mu$, we can write the integral as

$$\ell_r = r_\mu \int_{\chi_a}^{\chi_b} d\chi \sqrt{\frac{\chi}{1+\chi}}. \tag{49}$$

One can verify that the primitive of the integrand in this dimensionless integral is given by

$$\int d\chi \sqrt{\frac{\chi}{1+\chi}} = \sqrt{\chi}\,\sqrt{1+\chi} + \ln\Big(\sqrt{1+\chi} - \sqrt{\chi}\Big). \tag{50}$$

Note that this function is zero at $\chi = 0$. We therefore have for our integral

$$\ell_r \;=\; r_\mu \Big\{ \Big[\sqrt{\chi_b}\,\sqrt{1+\chi_b} + \ln\Big(\sqrt{1+\chi_b} - \sqrt{\chi_b}\Big)\Big] +$$

$$- \left[\sqrt{\chi_a}\,\sqrt{1+\chi_a} + \ln\Big(\sqrt{1+\chi_a} - \sqrt{\chi_a}\Big)\right]\Bigg\}. \tag{51}$$

In order to take the $r_\mu \to \infty$ limit, in which we have both that $\chi_a \to 0$ and that $\chi_b \to 0$, we first write this as

$$\begin{aligned} \ell_r &= r_b\,\frac{\sqrt{\chi_b}\,\sqrt{1+\chi_b} + \ln\big(\sqrt{1+\chi_b} - \sqrt{\chi_b}\big)}{\chi_b} + \\ &\quad -r_a\,\frac{\sqrt{\chi_a}\,\sqrt{1+\chi_a} + \ln\big(\sqrt{1+\chi_a} - \sqrt{\chi_a}\big)}{\chi_a}, \end{aligned} \tag{52}$$

where r_a and r_b are kept constant during the limit, so that we can write that

$$\begin{aligned} \lim_{r_\mu\to 0} \ell_r &= r_b \lim_{\chi_b\to 0} \frac{\sqrt{\chi_b}\,\sqrt{1+\chi_b} + \ln\big(\sqrt{1+\chi_b} - \sqrt{\chi_b}\big)}{\chi_b} + \\ &\quad -r_a \lim_{\chi_a\to 0} \frac{\sqrt{\chi_a}\,\sqrt{1+\chi_a} + \ln\big(\sqrt{1+\chi_a} - \sqrt{\chi_a}\big)}{\chi_a}. \end{aligned} \tag{53}$$

The limits of both terms on the right-hand side are now of the form $0/0$, so we use the L'Hôpital theorem and thus get for these limits

$$\begin{aligned} \lim_{r_\mu\to\infty} \ell_r &= r_b \lim_{\chi_b\to 0} \frac{\sqrt{\chi_b}}{\sqrt{1+\chi_b}} - r_a \lim_{\chi_a\to 0} \frac{\sqrt{\chi_a}}{\sqrt{1+\chi_a}} \\ &= 0. \end{aligned} \tag{54}$$

In particular, the whole proper radius of the inner vacuum region goes to zero in the limit. As a consequence, the inner vacuum has zero proper volume in the black-hole limit, despite the fact that its surface has a finite and non-zero proper area, associated to a non-zero apparent coordinate volume. One might even say that in the black-hole limits the inner vacuum region is not really there in any physically meaningful way. The same is the case for the inner region $[0, r_z]$.

Shifting now our attention to the temporal part of the geometry, let us discuss the $\pi_e \to \infty$ black-hole limits of $\nu(r)$, which we recall is the same as the $r_\mu \to \infty$ limit. From Equation (12) we have for the temporal coefficient of the metric in the inner vacuum,

$$\begin{aligned} \mathrm{e}^{2\nu(r)} &= \frac{1 - r_M/r_2}{1 + r_\mu/r_1}\,\frac{r + r_\mu}{r} \\ &= \frac{r_1}{r_2}\,\frac{r_2 - r_M}{r}\,\frac{r + r_\mu}{r_1 + r_\mu}. \end{aligned} \tag{55}$$

Taking the black-hole limit we get

$$\lim_{\xi_e\to\infty} \mathrm{e}^{2\nu(r)} = \left(\lim_{r_\mu\to\infty} \frac{r_1}{r_2}\right)\left(\lim_{r_\mu\to\infty} \frac{r_2 - r_M}{r}\right)\left(\lim_{r_\mu\to\infty} \frac{r + r_\mu}{r_1 + r_\mu}\right). \tag{56}$$

So long as we have that $0 < r \leq r_1$, the $r_\mu \to \infty$ limit of the last of the three factors above is just 1, so that we get

$$\lim_{\xi_e\to\infty} \mathrm{e}^{2\nu(r)} = \left(\lim_{r_\mu\to\infty} \frac{r_1}{r_2}\right)\left(\lim_{r_\mu\to\infty} \frac{r_2 - r_M}{r}\right). \tag{57}$$

Since in the black-hole limits we by definition have that $r_M \to r_{2\ominus}$, for all $r \neq 0$ the second limit above is zero, while the first one is some finite number, so that we get

$$\lim_{\xi_e \to \infty} \mathrm{e}^{2\nu(r)} = 0, \tag{58}$$

so long as $r \neq 0$, a result which corresponds to $\nu(r) \to -\infty$. There is therefore an infinite amount of red shift, with respect to asymptotic flat space at radial infinity, for all points within the inner vacuum, except for the origin. This indicates that close to the black-hole limit we have a radical slowing-down of the apparent time within all of the interior, as seen by an observer at radial infinity. Note that we still have the singularity at $r = 0$ in the black-hole limit, but that it is now a removable, strictly point-like singularity, where the temporal coefficient of the metric is positive and infinite, while it is zero everywhere else in a neighborhood of that point.

This result can be extended to the whole interior of the black hole, inside the event horizon. In fact, since by Equation (15) we have that in the matter region $F(r) > 0$, thus leading to $\ln[1 + F(r)] > 0$, and considering also that in the black-hole limits we have that $\nu(r_2) \to -\infty$, due to the singularity of $\nu(r)$ in the exterior Schwarzschild solution, it follow from Equation (12) that in the black-home limits we have that $\nu(r) \to -\infty$ in all the interior of the black hole, inside the event horizon at r_2.

The nature of the interior geometry that is obtained in the black-hole limits is way beyond our ability to imagine it in the usual visual way, and we must adhere only to the mathematics in order to be able to deal with it. The geometry is not embeddable in three dimensions in any simple way that could help us to form an intuitive visual understanding of it, in the way that is usually done for the exterior Schwarzschild geometry. But this is not all that there is to it, since we find ourselves here confronting a very strange and unexpected connection with results obtained by Prof. Gerard 't Hooft [8] from the study of the quantum mechanics for a naked black-hole, which is what we get, in any black-hole limit, for the exterior region of the black hole.

Two of the main results of that work seem to be the necessity for the identification of antipodal points of the horizon, and the absence of the interior of the black hole in any physically meaningful way. These two results map in an uncanny way onto the results that we get here, but in fact we get even more radical results here. While the results from [8] require only the identification of antipodal points, our results here imply that *all* points of the horizon are equally identified to one another. And even more than that, so are all the points of the interior as well. Regarding the effective absence of the interior, it maps onto the fact that the whole proper volume of the interior vacuum region is zero according to our results here. This will extend to the whole interior region behind the horizon in the case of the zero-temperature black-hole limits.

This identification of results becomes even more surprising and strange if we point out that while the results in [8] come from a quantum-mechanical analysis of the black-holes, our derivations here are entirely classical. They are no more and no less than the derivation and analysis of solutions to the Einstein field equations of General Relativity.

6 Concepts of Singularity

Despite the fact that the exterior Schwarzschild solution is valid only outside the position $r_M > 0$ of the event horizon, and only at radial spherical surface positions outside of which there is no matter at all, there seems to be a tendency to take seriously the curvature singularity at $r = 0$ that is displayed by this solution. One reason for this is that there is no such curvature singularity a the position of the horizon itself, since the singularity seen there is only a coordinate singularity. This means that it is possible to find alternative

systems of coordinates that display no singularity at all at that event horizon, making it possible, from the purely differential-geometric point of view, to consider connecting the inner and outer regions on either side of the horizon in a continuous and differentiable way.

However, these transformations of coordinates tend to interchange the roles of the temporal and radial (and hence spatial) coordinates. This is not physically reasonable, since the temporal and spatial coordinates are conceptually different from a physical point of view. While there is a fundamental symmetry between the temporal and spatial coordinates in General Relativity, we should not go so far as to claim that the temporal and a spatial coordinates can be simply interchanged, since they are such markedly different physical concepts. The invariance by coordinate transformations is fundamentally important, but so is the preservation of the signature of the metric, which identifies and differentiates the time coordinate. Therefore, physically acceptable coordinate transformations should not completely interchange the temporal coordinate with a spatial coordinate, or do anything that is equivalent to that.

None of this is an issue for our family of solutions here, since within this family event horizons never form, for any set of finite values of the free parameters of the family of solutions. When the black-hole limits are taken, leading to infinite values of π_e, we get a very definite, if strange and unexpected, resulting geometry within the horizon, just as we get the far more familiar Schwarzschild geometry in the region outside of it. However, while the geometry we obtain outside the horizon is the familiar one given by the exterior Schwarzschild metric right down to the event horizon, the one we get inside that surface has no relation at all to what the exterior Schwarzschild metric does inside that event horizon.

This suggests that a new definition of singularity is in order, one that takes into account the conceptual difference between temporal and spatial coordinates, as well as the preservation of the signature of the metric. One possible definition, that is based on very basic physical principles of the theory of Relativity, can be formulated as follows. An important concept of Relativity is that related to the invariance of events, in the sense that, if an event at a certain spatial point happens in a given system of coordinates, then it must happen at that same point in all other systems of coordinates as well. In other words, the *existence* of an event is a coordinate-invariant concept, which should be independent of the reference frame used to describe the events. This concept is often used in Special Relativity, even if it is not always explicitly stated, and it should be equally valid in General Relativity. Let us consider then a given solution of the Einstein field equations of General Relativity. We propose the following definition of a new type of singularity.

> If there is a spatial point in a solution of the Einstein field equations of General Relativity which is such that there exists an event at that point which happens in one reference frame but not in other reference frames, then that point should be considered as a singular point of the solution, on physical grounds.

In general this singularity does not have to be an invariant curvature singularity, and this new definition is proposed in *addition* to the usual one based on differential-geometric concepts, not as a replacement for it.

A simple example of this is any point at the event horizon of the exterior Schwarzschild solution, considered now as the boundary of that solution. It is a straightforward task to construct an event at such a point that exists in some reference frames, but does not exist in others. Just consider a material point particle falling freely in the radial direction towards the event horizon. As is well known, in the proper reference frame of the particle a finite proper time elapses from any arbitrary initial time to the time of the event "the particle arrives at the horizon". Therefore, in this reference frame the event happens at a finite time,

and therefore exists. However, when this same process is seen from a reference frame fixed at a very large radial distance, and as is equally well known, the time to that same event is infinite, and therefore the event never happens, and hence does not exist. Therefore, we should consider all points at the horizon as singular points in the new physical sense proposed here.

Given that the horizon is singular in this new sense, one should not expect that the exterior Schwarzschild solution has any physical meaning at all beyond that surface. Thus it is necessary to find other solutions that are valid in the whole spatial manifold, without these hard singularities of $\lambda(r)$ and $\nu(r)$ at that event-horizon surface. This is exactly what our new family of exact solutions does. Note that the physical impossibility of actually taking the black-hole limits within our family of solutions to their ultimate consequences, as discussed in Subsection 4.2, represents the physical impossibility of having actual singular points of this type in our family of solutions. The black hole solutions can be approached, but cannot be assumed. These limiting solutions can only be considered as simple approximate representations of physically very extreme solutions, not as exact and realizable physical solutions themselves.

7 Conclusions

In this paper we have completed the exploration, started in [5], of the parameter space of the new family of exact solutions of the Einstein field equations that was presented in [4]. This part of the exploration was dedicated to the asymptotic sub-regions of the allowed regions of the parameter planes of these solutions, for a few values of the polytropic index n. These are the regions where one can construct limits of solutions that approach the configurations of black holes. We have established the existence of many such black-hole limits within this region, in which limiting solutions containing event horizons are approached. We have also established that the new mass parameter μ, associated to the parameter r_μ that is introduced by the interface boundary conditions, diverges to infinity in all such limits.

There are, however, different types of such black-hole limits that can be considered. While in all of these limits the resulting exterior geometry, outside the event horizon, is always the same, namely the familiar exterior Schwarzschild geometry, as one would expect, the interior geometry is completely different from any expectations that one might have had, and depends, in its details, on the way in which the limit is taken. In some limits a shell of matter with non-zero proper thickness is left over, immediately within the horizon, and in other limits, those that lead to the matter being at zero local temperature, all the matter collapses completely to the position of the horizon. This leads, of course, to considerations involving the quantum behavior of the matter, which would prevent such a collapse.

Considerations involving the mathematical consistency of the solutions in the limits, the fact that there is a divergent energy in the limits, as well as the considerations involving the quantum behavior of the matter, all lead to the conclusion that the black-hole limits can be approached to a certain extent, but cannot be ultimately and completely taken. In any physically realizable situation there will always be matter in the vicinity of the position where the horizon would form. It is important to note that the presence of the repulsive singularity at the center has an important consequence regarding the possibility of the gravitational collapse of the matter. In any situation leading to such an event, the gravitational collapse will not happen inwards, towards the center, but rather towards the surface at the position of the formation of the event horizon, both from without and from within. Due to this, once more the region around the horizon never ceases to contain matter.

Independently of whether or not one takes black-hole limits, the geometry outside the position r_2 of the outer surface of the matter is always the familiar exterior Schwarzschild geometry. However, within that surface it is a completely different thing. In a general way, the difference can be described by pointing out the fact that, while outside the surface at r_2 the radial lengths are *stretched*, meaning that the proper lengths are larger than the corresponding variations of r, inside that surface the radial lengths are mostly *contracted*, meaning that the proper lengths are smaller than the corresponding variations of r. This is true for all radial positions to the left of the zero r_z of the function $\beta(r)$. This makes the interior geometry non-embeddable in the usual illustrative way used for the exterior Schwarzschild metric, and harder to understand intuitively.

In the black-hole limits the situation of the interior geometry becomes radically more extreme. As we saw in Section 5, in the whole region within the position of the zero r_z of $\beta(r)$, including the whole internal vacuum region, all proper radial distances between any pairs of points aligned along a radial direction simply collapse to zero. As a consequence, the minimum proper distance between any two points within this region, independently of whether or not they are aligned along a radius, all become zero. In other words, the physical distances between all pairs of points within a sphere at the position r_z become zero. From the point of view of the physics, all points in that regions become identified to one another. For all physical intents and purposes they are all one and the same point. Depending on the type of black-hole limit which is taken, this may or may not extend to the whole region within the horizon. For the zero-temperature limits the identification of all points does extend right up to the position of the horizon. For other limits, with non-zero local matter temperatures, there will be a thin shell within and right next to the horizon where there still are non-zero proper distances.

At this point we establish a surprising and unexpected connection to the results obtained by Prof. Gerard 't Hooft [8] from the study of the quantum mechanics for a naked Schwarzschild black-hole. As pointed out in Section 5, the two main results of that analysis, the identification of antipodal point of the horizon, and the physical absence of the interior of the black holes, can be easily and immediately interpreted in terms of the results that we get from the analysis of the interior geometry in the black-hole limits, in particular in the case of the zero-temperature limits. If anything, our results here are even more radical than those reported in [8]. Since in our case here, for the zero-temperature limits, all the points in the interior region of the black-holes turn out to be the same point, for all physical purposes, it follows that *all* the points at the horizon are completely correlated to one another, and hence this is valid in particular for the antipodal pairs of points.

In addition to this, as a consequence of our results for the interior geometry in the black-hole limits, it is easy to see that the proper volume of the interior of the black holes is zero. This volume is simply the sum of the proper volumes of concentric spherical shells, all of which have zero proper volume in the limit, since their proper thickness becomes zero. This is counter-intuitive and even bizarre, but follows unequivocally from the mathematics. In the limit the surfaces of the black-holes have finite and non-zero proper areas, but enclose zero proper volumes, even if there is a corresponding non-zero *apparent* coordinate volume. Hence, for all relevant physical purposes, we may conclude that the interior of the black hole is as good as absent. Whatever external perturbation is incident at one point of the surface of the event horizon, it has immediate effect on any other point of that surface, as if there was nothing else between them.

This relation with the results in [8] is that much more surprising since that work was done in the quantum domain, while our work here is entirely classical, in the sense that it is non-quantum in its intent. Is so far as we can tell at this time, there is no more in our work

here than the derivation and analysis of solutions to the Einstein field equations of General Relativity. However, this unexpected relation to the quantum results in [8] suggests rather strongly that there may be more to General Relativity than hits the eye. It suggests that there may be some underlying quantum structure to the theory of General Relativity, which somehow is intrinsic to it, if not immediately visible.

The fact that in all cases the interior geometry bears no resemblance at all to the behavior of the exterior Schwarzschild solution beyond the horizon, but is instead something completely different from that, leads to the definition of a new type of singularity, as explained in detail in Section 6. The definition proposed in that Section is based on the concept of the invariance of the *existence* of an event, which is a very fundamental concept of the theory of Relativity. The adoption of this new concept of singularity leads to the conclusion that the horizon is in fact the boundary of the region of physical validity of the exterior Schwarzschild solutions, and that there is no sense in trying to work out a differential-geometric or analytical continuation of that solution beyond that boundary, without reference to the matter that gives origin to the curvature of spacetime.

Acknowledgments

The author would like to thank Prof. Oscar J. P. Éboli for the use of the computer systems of his research group.

Data Availability Statement

Data sharing not applicable to this article as no datasets were generated or analyzed during the current study.

Conflict of Interest Statement

The author hereby certifies that there are no actual or potential conflicts of interest in relation to this article.

References

[1] K. Schwarzschild, "Über das gravitationsfeld eines massenpunktes nach der einsteinschen theorie (on the gravitational field of a mass point according to einstein's theory)," *Sitzungsberichte der Königlich Preussischen Akademie der Wissenschaften*, vol. 7, pp. 189–196, 1916.

[2] R. P. Kerr, "Gravitational field of a spinning mass as an example of algebraically special metrics," *Physical Review Letters*, vol. 11 (5), pp. 237–238, 1963.

[3] K. Schwarzschild, "Über das gravitationsfeld einer kugel aus inkompressibler flüssigkeit nach der einsteinschen theorie (on the gravitational field of a ball of incompressible fluid following einstein's theory)," *Sitzungsberichte der Königlich Preussischen Akademie der Wissenschaften*, vol. 7, pp. 424–434, 1916.

[4] J. L. deLyra and C. E. I. Carneiro, "Complete solution of the einstein field equations for a spherical distribution of polytropic matter," *General Relativity and Gravitation*, vol. 55, no. 5, 2023. Article ID: 67.

[5] J. L. deLyra, "The parameter planes of the spherically symmetric and static relativistic solutions for polytropes," 2023. DOI: 10.5281/zenodo.7871604.

[6] J. L. deLyra, R. de A. Orselli, and C. E. I. Carneiro, "Exact solution of the einstein field equations for a spherical shell of fluid matter," *General Relativity and Gravitation*, vol. 55, no. 5, 2023. Article ID: 68.

[7] P. A. M. Dirac, *General Theory of Relativity*. John Wiley & Sons, Inc., 1975. ISBN 0-471-21575-9.

[8] G. T. Hooft, "Black hole unitarity and antipodal entanglement," *Foundations of Physics*, vol. 46 (9), pp. 1185–1198, 2016.

A Full Set of Graphs

In this appendix we present full sets of graphs of each of the main observables determined in the exploration, for all 4 values of n and all the 8 values of τ_0 used, for all the black-hole limits considered. There are two general types of black-hole limit involved in these results. The first is the more basic type, leading to limits in which the matter has non-zero local temperatures. The second type of limit is characterized by a variable local temperature, leading to limits in which the matter has zero local temperature.

- In Figures A01 through A04 we show the behavior of the dimensionless length variable ξ_μ as a function of π_e, for the first type of black-hole limit considered. The heavy solid lines are linear fits to the last 100 point of each graph, which turn out to be perfect fits within the numerical precision used.
- In Figures A05 through A08 we show the behavior of the Energy Ratio E_R as a function of π_e, for the first type of black-hole limit considered.
- In Figures A09 through A12 we show the behavior of the Horizon Ratio E_R as a function of π_e, for the first type of black-hole limit considered.
- In Figures A13 through A16 we show the behavior of the Quantum Ratio Q_R as a function of π_e, for the first type of black-hole limit considered.
- In Figures A17 through A20 we show the behavior of the quantity $\ln(1 - E_R)$ as a function of $\ln(\pi_e)$, for the first type of black-hole limit considered.
- In Figures A21 through A24 we show the behavior of the quantity $\ln(1 - H_R)$ as a function of $\ln(\pi_e)$, for the first type of black-hole limit considered.
- In Figures A25 through A28 we show the behavior of the Quantum Ratio Q_R as a function of π_e, for the second type of black-hole limit considered.
- In Figures A29 through A32 we show the behavior of the quantity $\ln(1 - Q_R)$ as a function of $\ln(\pi_e)$, for the second type of black-hole limit considered.

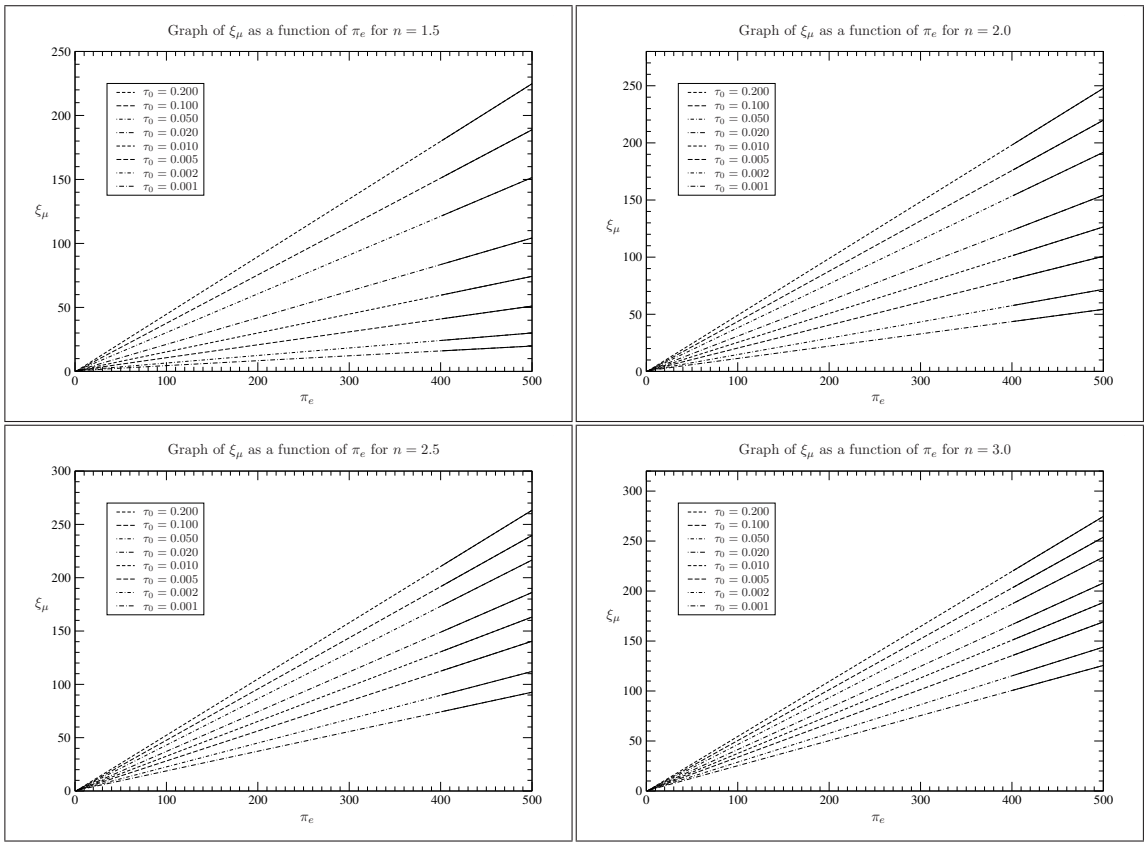

Figures A01–A04: The behavior of ξ_μ as a function of π_e.

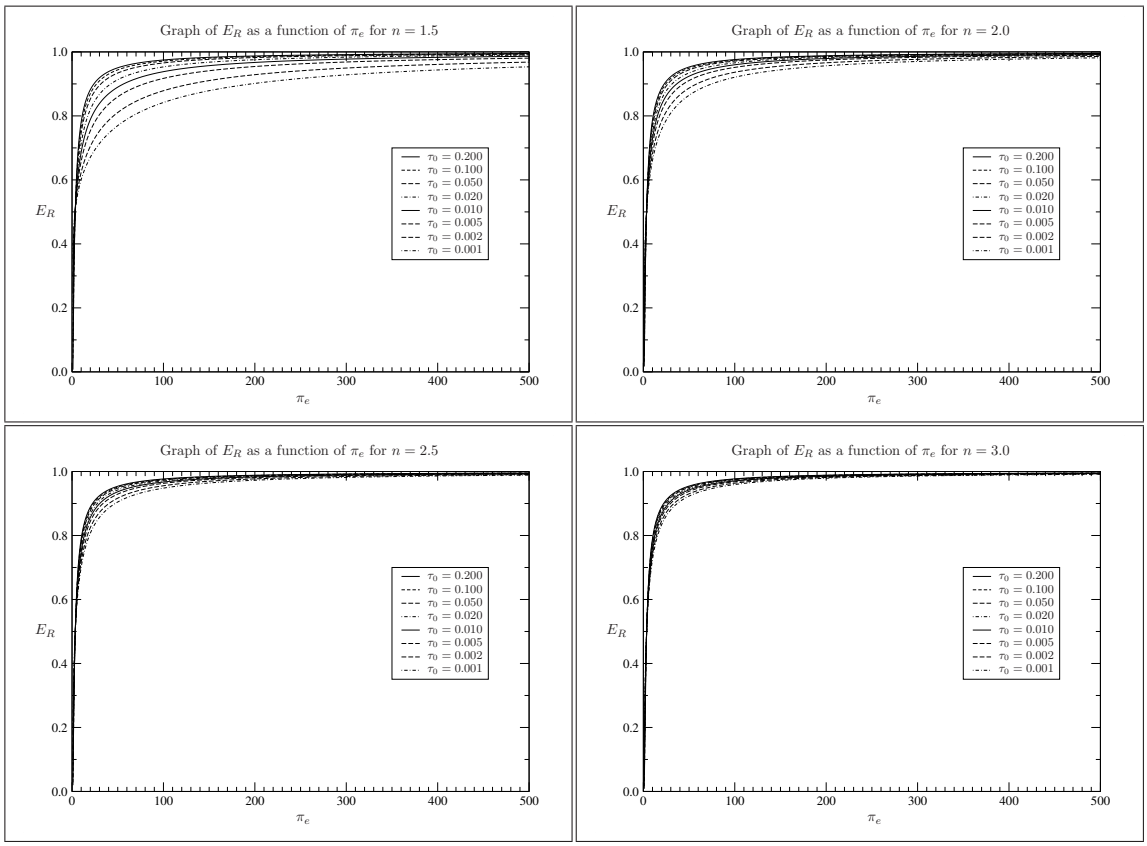

Figures A05–A08: The behavior of E_R as a function of π_e.

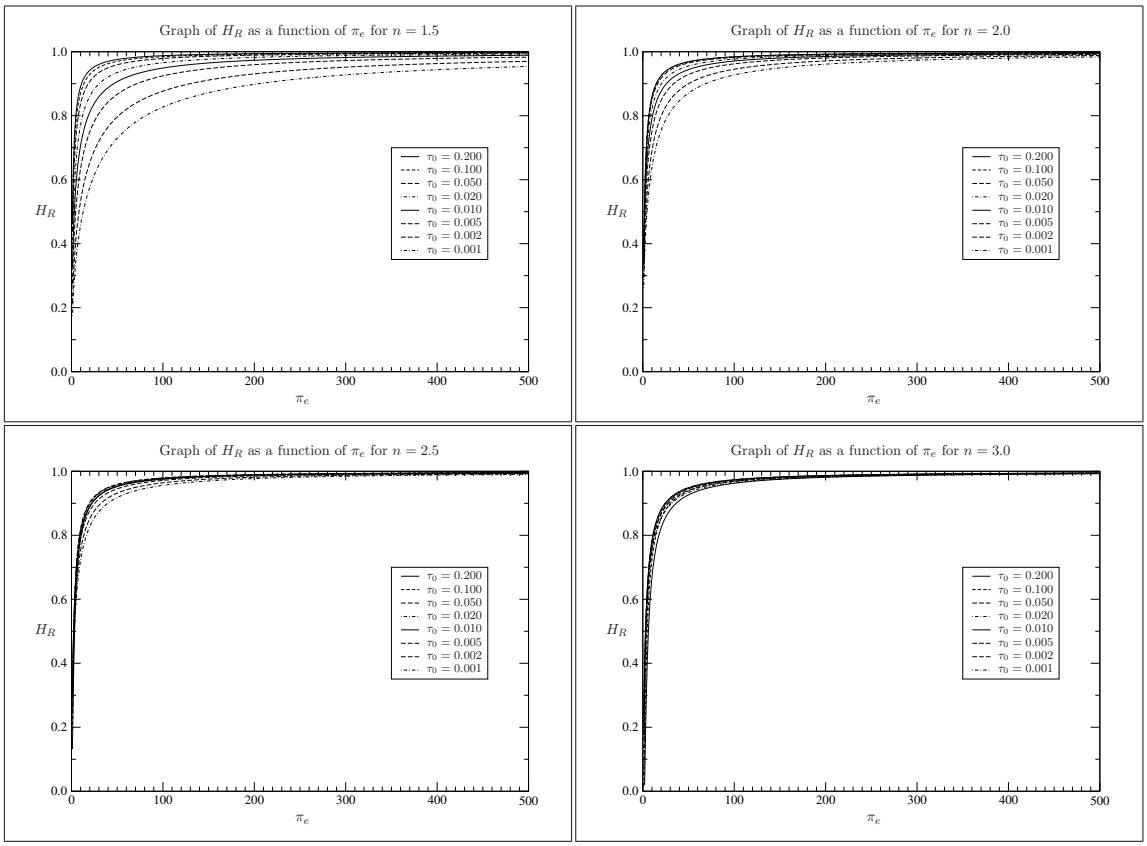

Figures A09–A12: The behavior of H_R as a function of π_e.

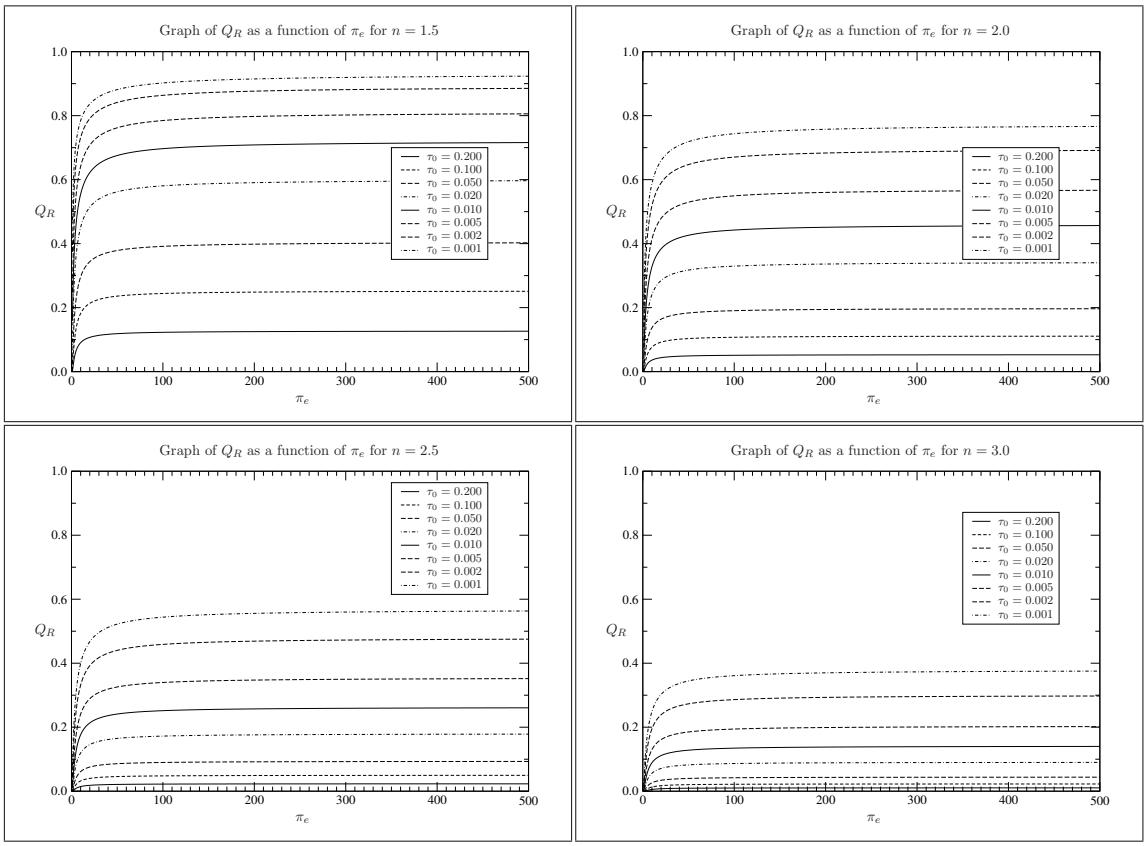

Figures A13–A16: The behavior of Q_R as a function of π_e.

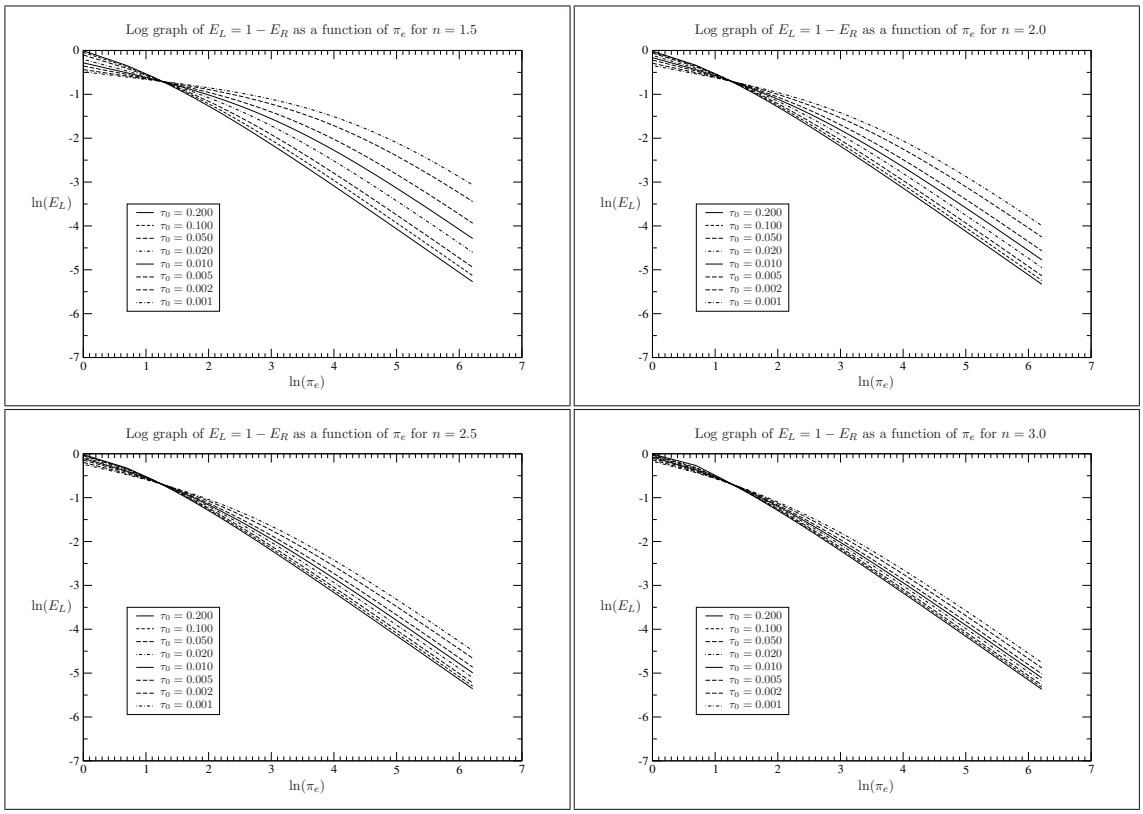

Figures A17–A20: Logarithmic plots of the behavior of $1 - E_R$ as a function of π_e.

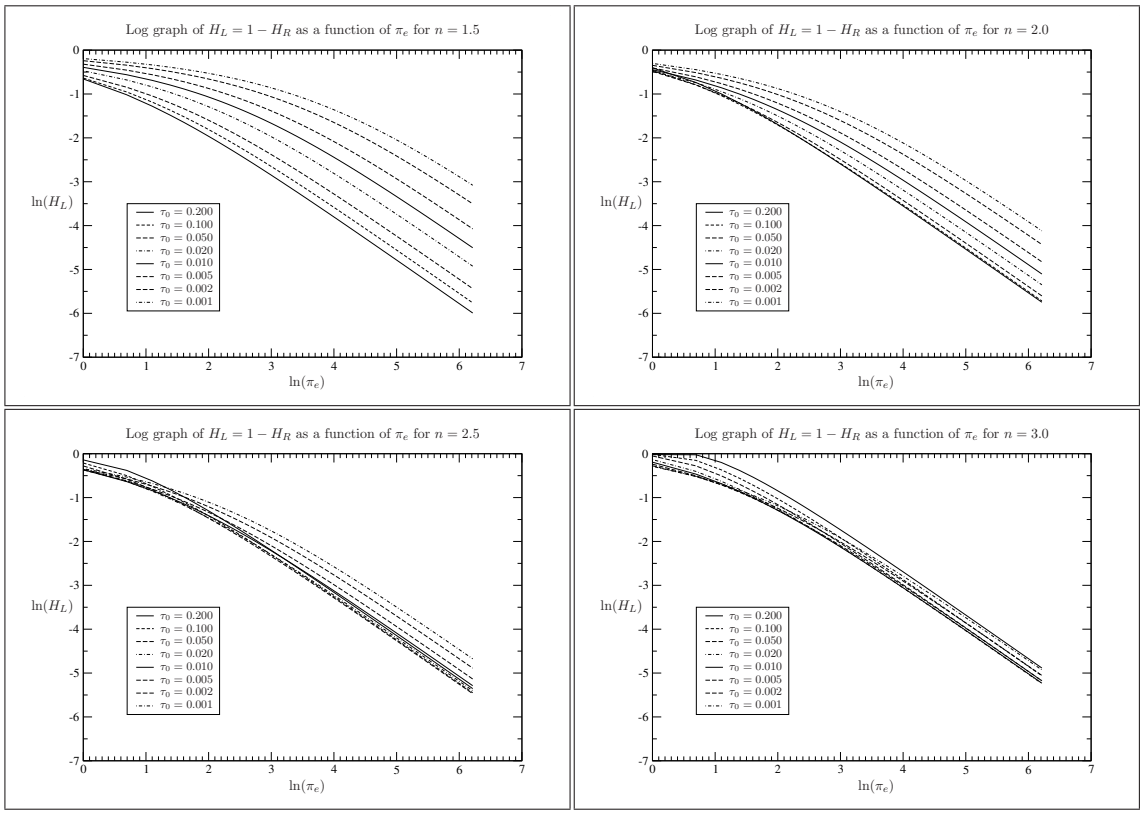

Figures A21–A24: Logarithmic plot of the behavior of $1 - H_R$ as a function of π_e.

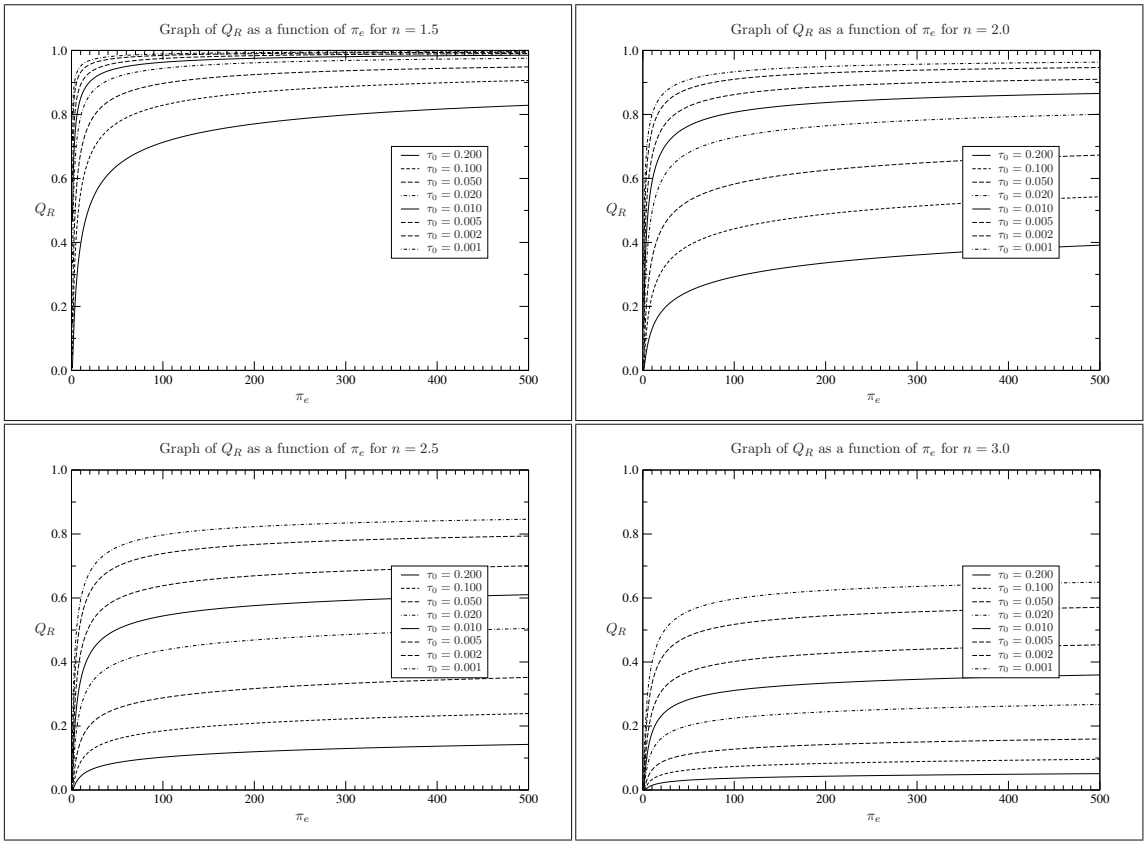

Figures A25–A28: The behavior of Q_R as a function of π_e, in the case of the second type of limit.

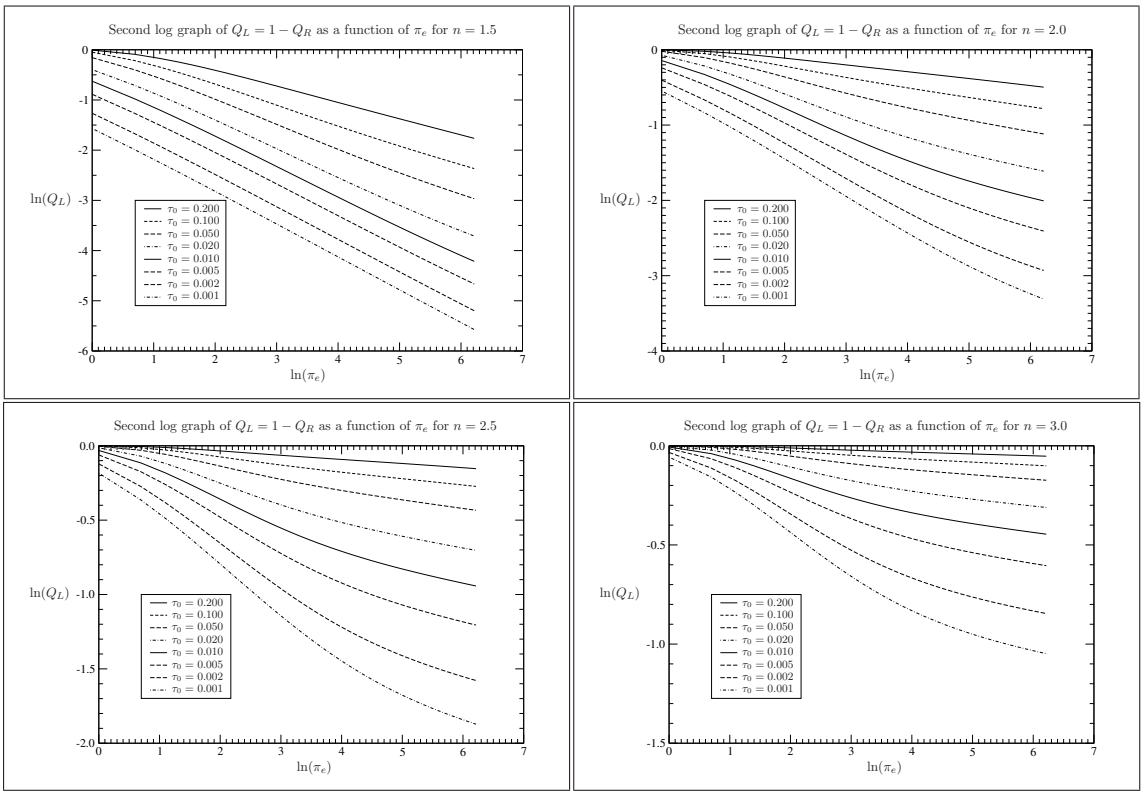

Figures A29–A32: Logarithmic plot of the behavior of $1 - Q_R$ as a function of π_e, in the case of the second type of limit.